CAPITAL UNIVERSITY OF SCIENCE AND TECHNOLOGY, ISLAMABAD


# Evaporation Dynamics of Drop-Drop and Drop-Wall Interaction

by

Muhammad Ahmed

A thesis submitted in partial fulfillment for the degree of Master of Science

in the

Faculty of Engineering
Department of Mechanical Engineering

2021

*This postulation is dedicated to my parents and teachers, who are constantly a light for me in obscurity and their unflinching help, guided my unfocused words into Sound thoughts*


# CERTIFICATE OF APPROVAL

## Evaporation Dynamics of Drop-Drop and Drop-Wall Interaction

by

Muhammad Ahmed

(MME 191005)

### THESIS EXAMINING COMMITTEE

| S. No. | Examiner | Name | Organization |
|---|---|---|---|
| (a) | External Examiner | Dr. Muhammad Anwar | IST, Islamabad |
| (b) | Internal Examiner | Dr. M. Javed Hyder | CUST, Islamabad |
| (c) | Supervisor | Dr. Muhammad Irfan | CUST, Islamabad |

Dr. Muhammad Irfan
Thesis Supervisor
December, 2021

Dr. M. Mahabat Khan
Head
Dept. of Mechanical Engineering
December, 2021

Dr. Imtiaz Ahmad Taj
Dean
Faculty of Engineering
December, 2021

# *Author's Declaration*

I, **Muhammad Ahmed** hereby state that my MS thesis titled "**Evaporation Dynamics of Drop-Drop and Drop-Wall Interaction** " is my own work and has not been submitted previously by me for taking any degree from Capital University of Science and Technology, Islamabad or anywhere else in the country/abroad.

At any time if my statement is found to be incorrect even after my graduation, the University has the right to withdraw my MS Degree.

**(Muhammad Ahmed)**
Registration No: MME 191005

# *Plagiarism Undertaking*

I solemnly declare that research work presented in this thesis titled "**Evaporation Dynamics of Drop-Drop and Drop-Wall Interaction**" is solely my research work with no significant contribution from any other person. Small contribution/help wherever taken has been duly acknowledged and that complete thesis has been written by me.

I understand the zero tolerance policy of the HEC and Capital University of Science and Technology towards plagiarism. Therefore, I as an author of the above titled thesis declare that no portion of my thesis has been plagiarized and any material used as reference is properly referred/cited.

I undertake that if I am found guilty of any formal plagiarism in the above titled thesis even after award of MS Degree, the University reserves the right to withdraw/revoke my MS degree and that HEC and the University have the right to publish my name on the HEC/University website on which names of students are placed who submitted plagiarized work.

**(Muhammad Ahmed)**
Registration No: MME 191005

# *Acknowledgement*

In the Name of Allah, The Most Gracious, The Most Merciful. Praise be to God, the Cherisher and Sustainer of the worlds. All thanks to Almighty Allah, The Lord of all that exist, who bestowed me with His greatest blessing i.e. knowledge and Wisdom to accomplish my task successfully.

Thousands of salutations and benedictions to the Holy prophet Hazrat Muhammad (PBUH) the chosen-through by whom grace the sacred Quran was descended from the Most High. I am very thankful to Dr. Muhammad Irfan, a great teacher, mentor and supervisor who made a difference in all aspect of my life. I am indebted to Dr. Muhammad Irfan for his valuable guidance, encouragement and dedicated support that enabled me to complete my MS Degree Program.

I want to express my heartiest regards to my parents who always supported me morally, spiritually and prayed for my success.

**(Muhammad Ahmed)**

# *Abstract*

Moving droplets evaporation in a gas environment is frequently encountered in many engineering applications including cooling towers, flash spray, spray combustion, spray drying, spray cooling, fire suppression, and liquid atomization. For many years, the researchers' attention focused on the atomization of the liquid. Atomization of liquid is mainly divided into two types: primary and secondary atomization. Spray nozzles, flow in compressors and capillaries, etc., are examples of primary atomization. On the other hand, droplet collisions with each other or with the wall are considered secondary atomization. To understand the spray cooling, spray drying, fuel injection in aircraft engines and internal combustion engines, the interpretation of relevant basic processes such as drop coalescence, single droplet impact, and drop-on-drop collisions, etc., is required. The present work focuses on the evaporation dynamics of interacting droplets and a droplet impacting over a heated wall.

A commercial CFD software ANSYS Fluent is used to simulate the drop-drop evaporation in a saturated vapor (single component) medium. The model is validated for both single and multiple droplets with the results available in the literature. During the study normalized $d^2$, droplet trajectory, and droplet velocities are considered important parameters. Simulations on in-line and lateral configurations are then carried out by varying spacing between them and, the effect on normalized $d^2$, trajectory, and velocities are analyzed. Later on, in inline configuration, the effect of two arrangement patterns is examined: the small-big arrangement (SBA)and the big-small arrangement (BSA). In SBA, a small droplet is a trailing droplet and a big droplet is a leading droplet. Whereas in BSA big droplet is a trailing and a small droplet is a leading droplet. The drop-drop coalescence is more intensive for the BSA of droplets as compared to SBA. It is also observed that in the SBA, overall evaporation is faster as compared to BSA. In BSA trailing drop dominates the coalescence process because of its larger size, higher rising velocity, and stronger velocity field. It is also observed that for the SBA when the sizing ratio is increased from 0.5 to 0.9 the normalized $d^2$ of the leading droplet remains the same whereas in the trailing droplet slow down in evaporation is noticed due to effect of thermal buffer layer.

In the second step, numerical simulations are performed to analyze the evaporation dynamics of the droplet impinging on a heated wall. The model is validated using the experimental and numerical observations of FC-72 single droplet impact over the heated chromium surface. In the validation, spread radius, and heat flow is compared and good results are observed. Next, the impact velocity, drop size, wall temperature and boundary layer thickness are varied and the effect on heat flow and spread radius is investigated. It is found that higher wall superheats, higher impact velocities, or larger drop diameters results in increasing heat flow after the impact. With the increase in boundary layer thickness, a negligible decrease is noticed on heat transfer during receding phase. The maximum spreading radius after impingement increases with increasing impact velocity or impact diameter and no effect with rising wall superheat, thermal boundary layer thickness because of constant wettability of the surface.

**Keywords:** *Droplet, arrangement pattern, drop-drop interaction, drop-wall interaction, droplet evaporation, size ratio, VOF, sprays*

# Contents

# List of Figures

# List of Tables

# Abbreviations

| | |
|---|---|
| **BSA** | Big-small arrangement |
| **Bo** | Bond number |
| **Eo** | Eötvös number |
| **FC-72** | Perfluorohexane |
| **Ja** | Jakob number |
| **LD** | Leading droplet |
| **Mo** | Morton number |
| **Pr** | Prandtl number |
| **Re** | Reynold number |
| **SBA** | Small-big arrangement |
| **TD** | Trailing droplet |
| **We** | Weber number |

# Symbols

| | |
|---|---|
| $d$ | drop diameter |
| $d_o$ | drop initial diameter |
| $u_o$ | drop initial velocity |
| $\eta$ | density ratio |
| $\lambda$ | viscosity ratio |
| $\alpha_l$ | liquid volume fraction |
| $\alpha_v$ | vapor volume fraction |
| $\rho_l$ | liquid density |
| $\rho_v$ | vapor density |
| $\dot{m}_l$ | mass dissipated by liquid phase |
| $\dot{m}_v$ | mass gain by vapor phase |
| $F_v$ | volume force due to surface tension |
| $\kappa$ | interface curvature |
| $h_{lv}$ | latent heat of vaporization |
| $K_l$ | themal conductivity of liquid phase |
| $K_v$ | themal conductivity of vapor phase |
| $T_l$ | liquid temperature |
| $T_v$ | vapor temperature |
| $T_{wall}$ | wall temperature |
| $\theta$ | contact angle |
| $\hat{n}_w$ | normal unit vector to wall |
| $\hat{n}_t$ | tangential unit vector to wall |
| $R$ | Size ratio |
| $S$ | initial distance ratio |

| | |
|---|---|
| $S_x$ | initial distance ratio for lateral drops |
| $S_y$ | initial distance ratio for inline drops |
| $L_x$ | distance between the centroids of two laterally arranged drops |
| $L_y$ | distance between the centroids of two axially arranged drops |
| $g$ | gravitational acceleration |
| $\sigma$ | surface tension force |
| $\mu_g$ | viscosity of gas/vapor |
| $C_{p,g}$ | specific heat of gas |
| $T_{sat}$ | saturation temperature |
| $h_{lg}$ | latent heat of vaporization |
| $Sp$ | spreading ratio |
| $T_o$ | Degree of superheat |
| $C$ | courant number |
| $r_{cl}$ | spreading/ contact line radius |
| $\delta t$ | thermal boundary layer thickness |
| $e$ | distance from drop centroid to its side wall |

# Chapter 1

# Introduction

## 1.1 Background

Multiphase flows, which are widely observed in nature, have gathered significant attention in the past few decade due to their engineering and technical application such as in fire suppression, heat exchanger, wastewater treatment, spray drying, fogs, mist, etc. Multiphase flows are categorized into four types [1] liquid-gas, liquid-solid, gas-solid, and three-phase flows. Fuel injection systems in gas turbines, internal combustion engines, inkjet printing, spray painting and cooling systems are some examples of gas-liquid flows.

Figure 1.1 represents the whole injection or evaporation system in a diesel spray. In a diesel spray when liguid enters in a combustion chamber with high velocity or pressure, jet break up is observed according to the mechanism of atomization. Two distinguish zones within the jet that are dominated by different phenomena are observed. Close to the nozzle the liquid jet breaks up into larger drops and primary breakup happens this is called primary atomization. Then these big drops further break down into smaller and smaller droplets as a result of secondary atomization. Primary and secondary atomization regions are dominated by liquid inertia and surface tension. After the secondary breakup, the surface area of the drop becomes large and the effect of evaporation dominates the flow.The present work focuses on droplet evaporation after secondary atomization, where drop-drop and drop-wall interaction take place.

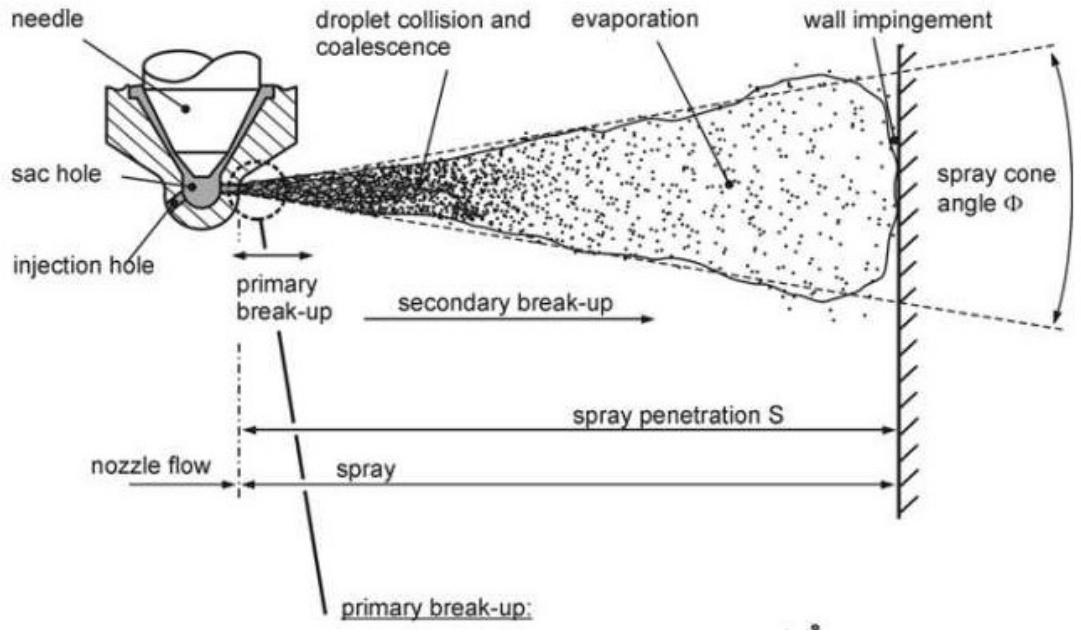


FIGURE 1.1: Atomization in diesel spray [2]

## 1.2 Fundamentals of Binary Droplet Collision

The majority of early work related to two droplet collisions dates back to the 1960s. Gunn [3] identified four typical scenarios that arise due to binary water droplets collision bouncing, coalescence, drop disruption and, drop spatter as shown in Figure 1.2. The collision of multiple droplets is a very complex process, the participating droplets may have different materials or sizes which are miscible or immiscible. Variation of the surface tension, droplet evaporation, and burning significantly affect the droplet collision.

Qian and Law [4] and Li and Fritsching [5] have classified the collision outcomes in various categories. The qualitative collision regimes are shown in Figure 1.3 and vary differ with different We, Re, density, and viscosity ratios without considering other effects as given by the function below:

$$B = B[Re, \eta, \lambda]$$

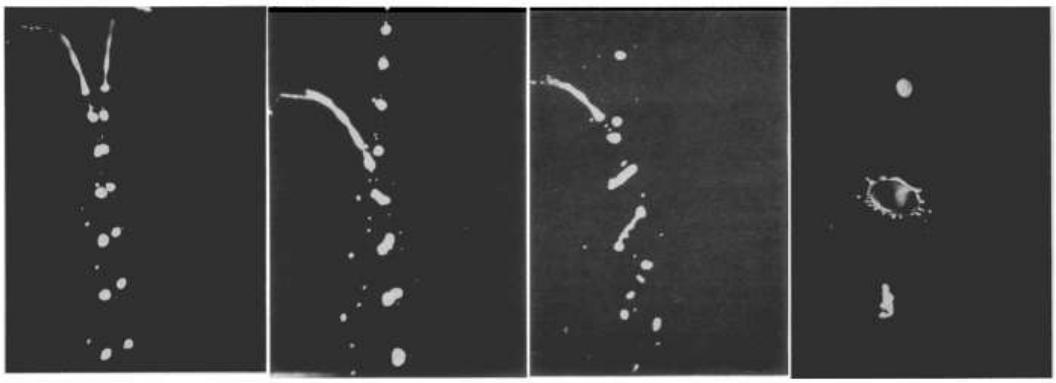

FIGURE 1.2: Water droplet collision characteristic [3]. From left to right: bouncing, coalescence, distruption after coalescence and drop spatter

For binary droplet collision, five major distinct regimes were observed named as (I)coalescence with minor deformation, (II)bouncing, (III)coalescence with major deformation, (IV)reflexive separation, and (V)stretching separation as shown in Figure 1.3. In regime, I and III the two droplets merge to form a larger drop. In regime I the droplet have adequate time to expel the intervening gas due to low weber number, then the drops coalesce permanently with small deformation. On the other hand in regime III gas layer between drops rupture due to increase in kinetic energy and coalescence with major deformation occurs. In regime II, with an increase in weber number, the time for drainage of a gas layer between droplets is short due to which two drops collide and separate without merging this regime is known as bouncing. In regimes, IV and V reflexive and stretching separation occurs. In reflexive separation, head-on or nearly head-on collision between droplets occur whereas, in stretching separation, there is an off-axis collision between droplets and form an elongated liquid filament. As droplets retract, it results in the formation of multiple satellite droplet. Formation of child droplets increase the surface area of liquid, with increase in surface area ultimately there is an increase in evaporation rate.

In evaporation, droplet surface area exposed to high-temperature gas plays a significant role. In coalescence when two or more drops merge and form a new drop, the formation of a big droplet decreases the surface area exposed to high-temperature gas as compared to two initial droplets. It results in a decrease in the evaporation rate. Similarly in stretching and reflexive separation formation of

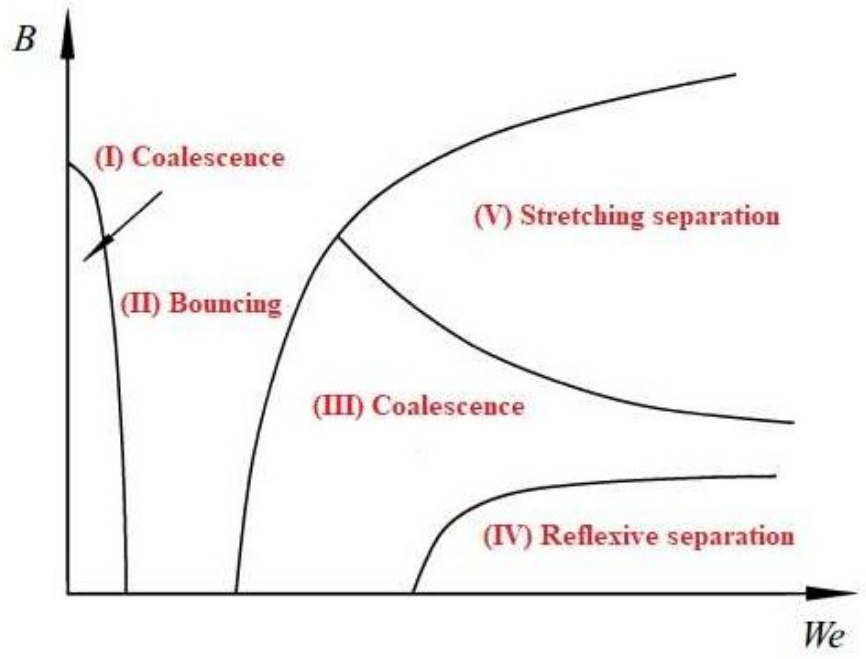


FIGURE 1.3: Schematic of various collision regime [5]

child droplets increase the evaporation rate as compared to two initial droplets

## 1.3 Fundamentals of Droplet Impingement

Understanding the impact of droplets on the solid surface is important because of its numerous industrial and technical applications such as ink-jet printing, direct and indirect injection systems, microprocessor cooling, and fire suppression.

The phenomena of the drop impingement process significantly differ from case to case depending on the various parameters characterized in Figure 1.4 which result in different outcomes. At the time of impact, it is possible that drop might be spherical, deformed, or elliptic. The impact may be oblique or normal, in the air or a vacuum. The drop may impact on the wall, solid surface, free surface of liquid on a thin film or in a deep pool. The solid surface may be soft or hard, smooth or rough, chemically heterogeneous or homogeneous, it may also curve, flat or porous. The temperature of the drop may be same or different from the wall. The liquid of the drop can be Newtonian or non-Newtonian. In addition, the

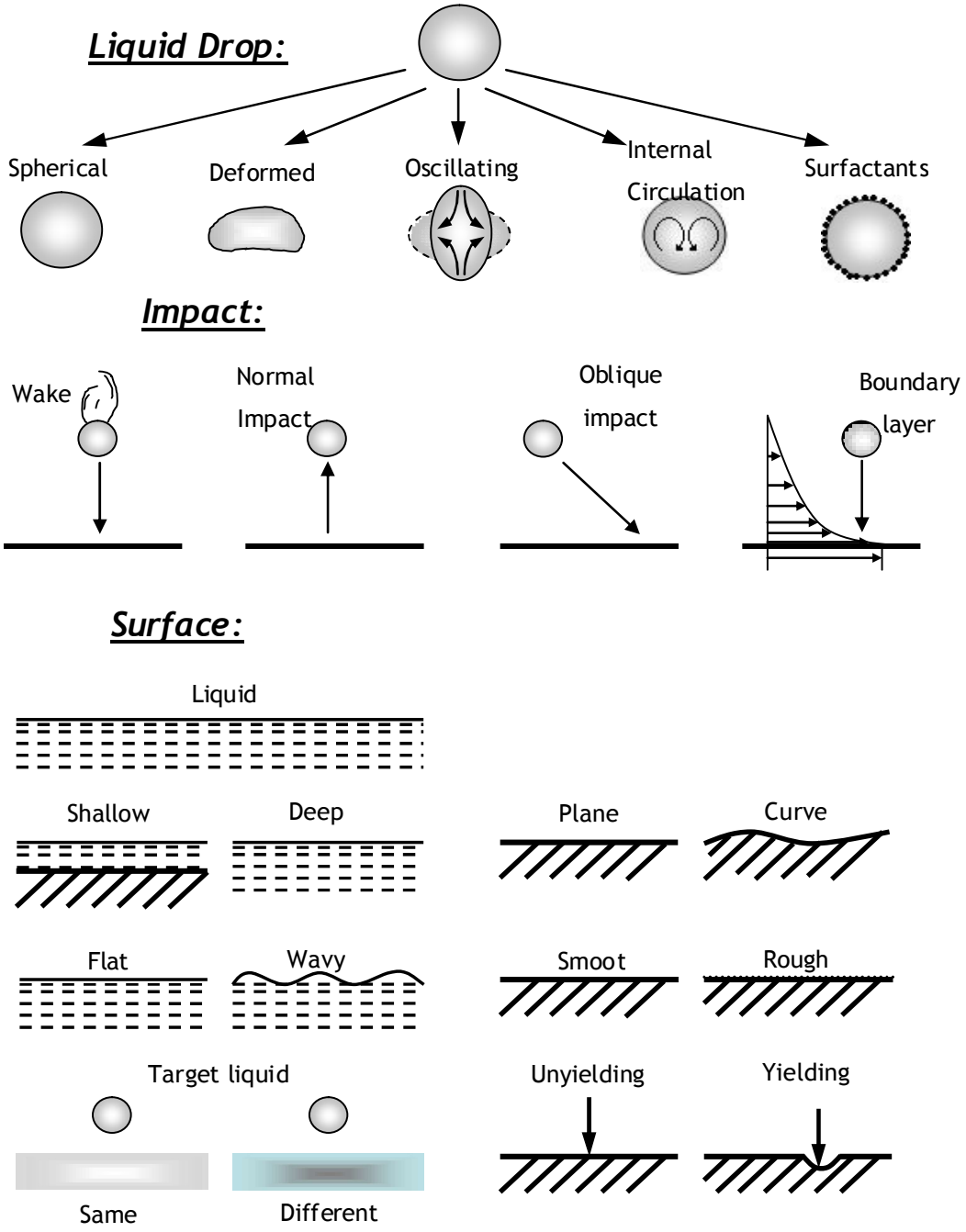


FIGURE 1.4: Classification of possible drop impingement scenarios [6]

outcome of drop impact depends on its direction relative to the surface, the impact velocity, drop size, the properties of the drop, the wettability and roughness of the solid surface, the non-isothermal effects (e.g., evaporation and solidification), and air entrapment. Flow pattern are substantially affected by the pre-existing or generated waves on liquid surface. The impact may result in the drop spreading,

receding, rebounding, or even levitating if the evaporation rate near a hot wall is strong for the Leidenfrost effect.

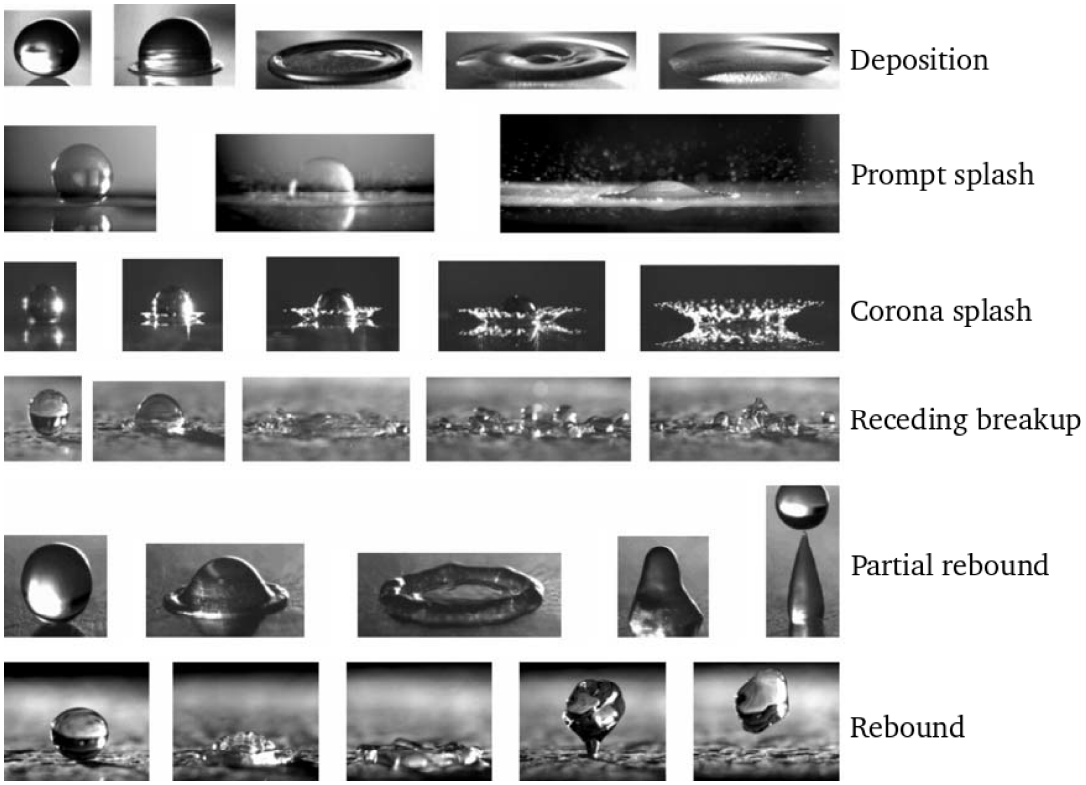


FIGURE 1.5: Possible morphologies of drop impingement onto drywall [7]

Droplet behavior during impingement is significantly affected by the surface properties of the wall and the impingement parameters. For this a systematic classification of the scenarios which can be observed in Figure 1.5 has been worked out by Yarin [8] and Rioboo et al.,[7]. If the inertia of the droplet is small compared to viscous forces then the so-called droplet deposition will be observed and it is shown in first row of Figure 1.5. In this regime, no instabilities are observed and no secondary droplets will be created during the impingement process. If the inertial forces of the droplet are dominating as compared to viscous forces there is prompt and corona splash is observed. During the receding phase, if there is a droplet splash with the generation of satellite drops it is prompt splash if the rim shape form of droplet then the corona splash can be seen. A receding breakup is noticed for superhydrophilic/completely wetting surfaces. A partial rebound with secondary droplets ejecting out of the droplet during the receding of the droplet if

the surface is hydrophobic/partially wetting. A complete rebound from the surface is observed for the superhydrophobic/ completely non-wetting surface.

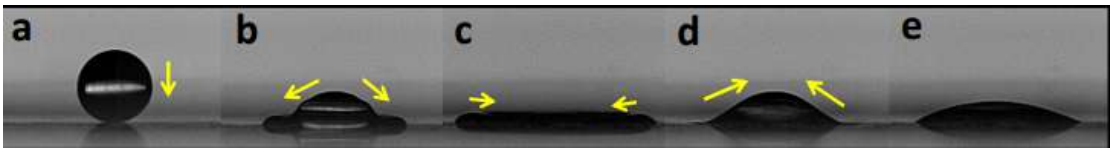


FIGURE 1.6: Behaviour of impinging droplet (a) Pre-impacting droplet (b) Advancing phase (c) Maximum spread (d) Receding phase (e) Sessible droplet [7]

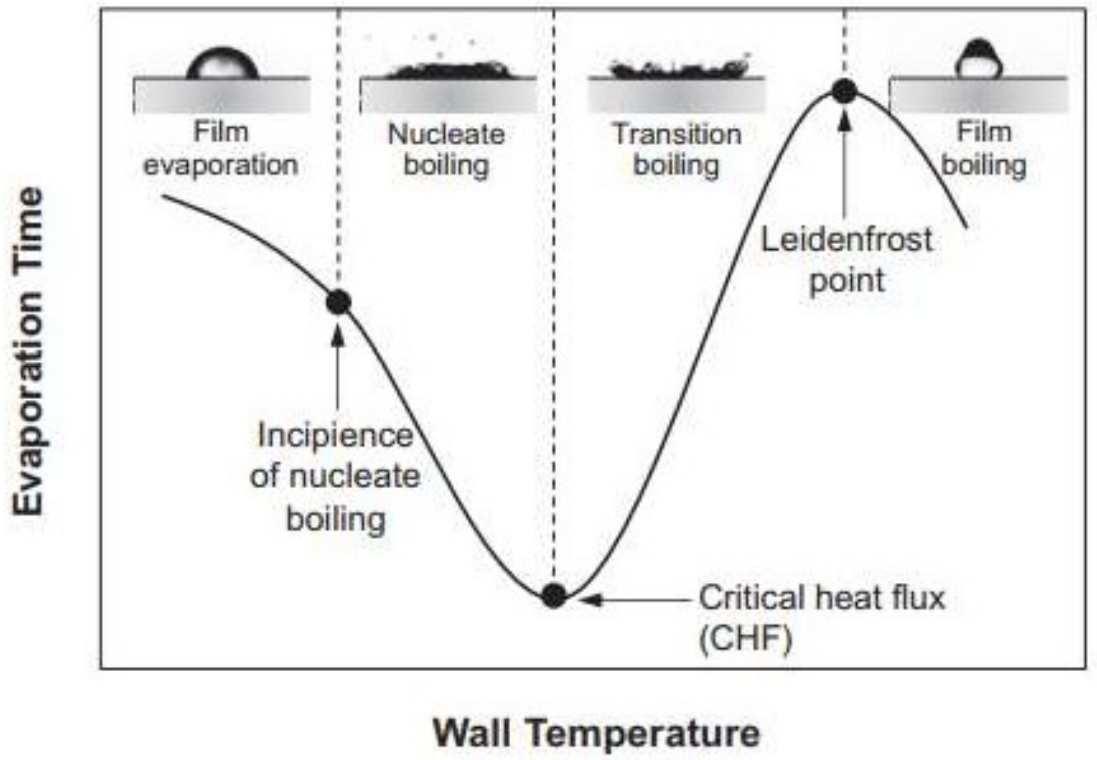


FIGURE 1.7: Evaporation regimes associated with a droplet impact on a hot wall [9]

When a droplet is impacted on a surface, it will perform cycles of the advancing (spreading) and receding (retracting) phases for a specific time and comes to a static position, which is named the sessile droplet.

Figure 1.6 shows the hydrodynamics observed during one cycle of post-impingement behavior, and the sessile droplet. During the advancing phase, [7] the inertial forces influence the spreading, and droplet spreads to a maximum due to viscous dissipation. At this point, the capillary forces dominate and retract the droplet.

A series of cycles will continue until it dissipates the energy and reaches an equilibrium (sessile droplet).

When cool droplet impacts on heated surfaces, the mean temperature of liquid increases and evaporation occurs. Depending on the wall temperature, four different evaporation regimes can be observed as shown in Figure 1.7. There are film evaporation, nucleate boiling, transition boiling, and film boiling.

Film evaporation happen when wall temperature is greater or equal to saturation temperature but insufficient to initiate bubble in nucleation. In film boiling regime, liquid spreads on the hot wall and starts to become thin due to the evaporation effect. In nucleate boiling, bubble formation occurs at the nucleation site. The nucleate boiling region extends from the incipience of bubbles to the critical heat flux (CHF) which corresponds to the shortest drop lifetime. Immediately after critical heat flux, boiling become unstable and transition boiling occur. The intermediate regime between critical heat flux (CHF) and leidenfrost point is the transition regime. In the transition regime, a high density of bubbles cover the wall which acts as insulation. Due to the lower thermal conductivity value of vapor film as compared to liquid, boiling becomes unstable. As a result increase in wall temperature also increase the evaporation time. Impingement of liquid drop in film boiling regime is also known as leidenfrost phenomena.

## 1.4 Scope and Objective of this Work

In the present study, dynamics of droplet evaporation during secondary atomization, where drop-drop and drop-wall interaction occurs, are investigated.

In drop-drop interaction numerical model is first validated with the numerical observations available in the literature [10]. Following that, inline and lateral configurations under the same impact conditions are investigated. Further, in inline configuration, the effect of size ratio on small-big arrangement (SBA) and the big-small arrangement (BSA) is investigated. This arrangement enables us to understand the evaporation dynamics of differently sized interacting droplets.

For drop-wall Interaction numerical model is first validated with the available numerical [11] and experimental observations available in the literature[12]. First

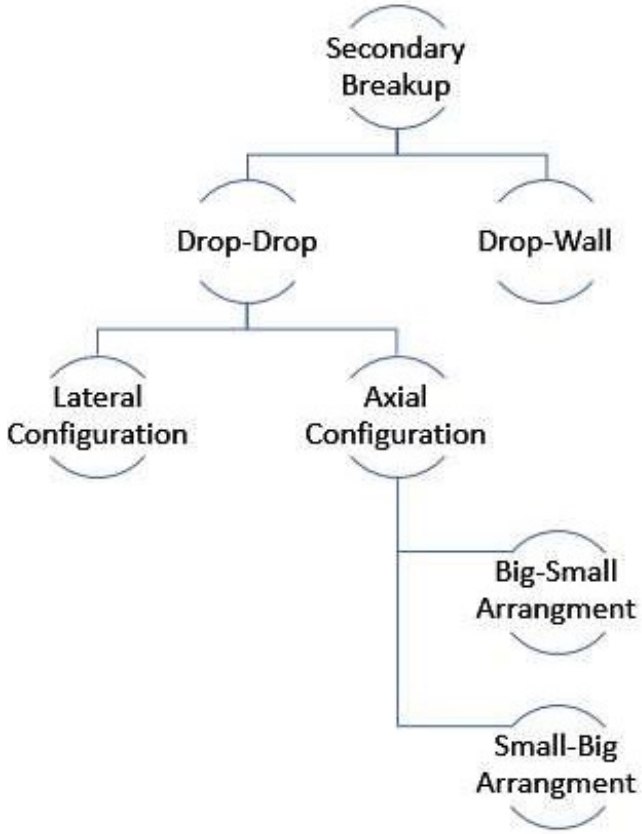


FIGURE 1.8: Systematic layout of the studied configuration

hydrodynamics and global heat flow behavior of drop-wall interaction is studied Further in drop-wall interaction, the effect of drop velocity, size, and boundary layer thickness on the contact line radius and heat transfer is examined. Figure 1.8 presents the studied configuration in the form of a flow chart.

## 1.5 Thesis Outline

The thesis is organized into six chapters. A short description of the contents of each chapter is given below:

**Chapter 1** provides a brief introduction to the motivation/background of the present work. It also includes the scope and objective of this work.

**Chapter 2** presents a detailed literature review related to numerical and experimental investigation of the drop-drop and drop-wall interaction. Subsequently, the key findings of the literature are discussed in detail and the research gap is

identified.

**Chapter 3** is about the mathematical modeling of drop-drop and drop-wall interaction.

**Chapter 4** provides the details of numerical investigation of drop-drop interaction in saturated vapor medium and results are thoroughly discussed.

**Chapter 5** provides the details of numerical investigation of drop-wall interaction in saturated vapor medium and results are discussed.

**Chapter 6** presents the conclusions of this research study. This chapter also consists of the future recommendations in the area of study under consideration.

# Chapter 2

# Literature Review

This chapter deals with a critical literature review pertinent to the numerical and experimental investigation of drop-drop and drop-wall interaction. For ease of reading, the literature review is discussed under the following headings.

## 2.1 Studies on Drop-Drop Interaction

In many industries, binary droplet collision is important, for example, combustion, sintering process, coating, printing, and food processing. The droplet collision, as well as its frequency, will affect the heat and mass transfer.

In the past few decades, many studies have focused on vaporization and combustion of single droplets either in a stagnant or convective flow environment [13]–[15]. Kuznetsov et.al., [16] experimentally studied the evaporation of water droplets of size 1-2.5 mm in high temperatures up to 1100°C. It was recorded that evaporation and heating of free-falling droplets occur more rapidly as compared to droplets that rest on the holder. The presence of neighboring droplets significantly affects the vaporization and burning rates of droplets. Recognizing the importance of droplets interaction some researchers devoted their studies to the collision of multiple droplets and its effect on evaporation and surface area. Chen et.al., [17] investigated the dynamics and outcomes of the mass transfer process of different sized binary water droplets collision in atmospheric air with size ratios 0.5 and

0.25. During the study, it was indicated that mass transfer ratio is weakly dependent on Weber number but has a strong effect on impact parameter. Daisuke et.al., [18] experimentally examined the effect of droplet spacing on 13 fuel droplet clusters in microgravity condition. During the work it was observed that, with a decrease in droplet spacing initial heat-up time increases and the rate of evaporation after the initial heat up was constant. In order to quantify the effect of the droplets interaction on normalized $d^2$, Sherwood number and Nusselt number is investigated by Deprédurand et.al., [19]. Numerous experiments were performed using monodisperse fuel droplets having different volatilities. The experimental Sherwood and Nusselt number were then compared with isolated drops and concluded that these numbers are dependent on the interaction between the droplets in a same way as it depends on the fuel nature. In [20] Shlegel et.al., studied four regimes of droplet collision: coalescence, bounce, disruption and separation at 20°C and interaction regime map was plotted for the water droplet collision accounting for the linear interaction parameter and the Weber number. Further Shlegel et.al., [21] studied effect of the initial temperature of the water droplets on their interaction regime. Shlegel et.al., [21] concluded that the ratios of the free surface areas of the newly formed fragments increased 10% for droplet temperature 90°C as compared to droplet when their temperature was 20°C. The main advantage of formation of large number of small droplets was that they evaporate more quickly as compared to two initial droplets

Volkov et.al., [22] experimentally investigated the evaporation of two water droplets moving sequentially one after the other in the high temperature combustion environment. The results were also compared with the theoretical prediction. During the work it was found that if the tandem distance L between the droplets is greater than 8, then the effect of evaporation of the leading droplet on the trailing droplet become insignificant. Further Volkov et.al., [23] extend their study to the evaporation of falling droplets in series of 2,3 and 4. The influence of drop size, spacing between drops, drop temperature and their numbers during motion were investigated on the intensification of evaporation. Yang et.al., [24] numerically investigate the combustion of two fuel droplets by using the VOF model with different droplet radii and initial center. It was found that the burning rates of the

front droplet are always greater as compared to back droplets.

To the best of the author's knowledge, numerical simulation on heating and evaporation of two different sized interacting droplets has not been performed yet. The main novelty of this research work is to investigate the evaporation dynamics of two different-sized interacting droplets. We select droplet size ratio and the two arrangement patterns small–big arrangement (SBA) and big–small arrangement (BSA) for investigation. In SBA, the small droplet is a trailing droplet and the big droplet is the leading droplet. Whereas in BSA big droplet is trailing and a small droplet is a leading droplet.

## 2.2 Studies on Drop-Wall Interaction

Most of the initial studies were devoted to single droplet impact on isothermal surfaces. As the impacting phenomena are also important in internal combustion engines, spray painting, inkjet printing, and coating applications. From earlier studies conducted on droplet impingement over adiabatic surfaces, the droplet impact scenario is categorized into three types based on the nature of the target, i.e., liquid film, deep liquid pool and solid wall. In the case of droplet impingement over hot surfaces, the process involves heat and mass transfer interactions and requires additional efforts for a better understanding of the phenomenon. A comprehensive review of studies concerning the droplet impact on a heated wall is presented by Liang and Mudawar [9].

In 1991, Chandra and Avedisian [25] experimentally investigated the droplet impingement of n-heptane liquid droplets over a dry heated stainless steel surface using the flash photographic method. During the study, boiling regimes from film evaporation up to the Leidenfrost point were observed. It was found that inside the droplet numerous bubbles were formed at high temperatures, but below the Leidenfrost point the formation of the bubble does not affect the overall droplet shape. Lee et.al., [26] conducted the experiments to investigate the droplet impact of PF-5060 over a hot surface with the degree of superheat of 9K,19K, and 29K by keeping the drop diameter and impact velocity as fixed. The heat flux and deformation were considered important factors. It was observed that the heat

transfer coefficient is dependent on droplet spread. Börnhorst and Deutschmann [27] experimentally investigated the impinging behavior of an aqueous urea solution. The effects of surface temperature, impact velocity, and droplet diameter are key parameters of the investigation. Four interaction regimes depending on thermal parameters and hydrodynamics that is deposition, splash, boiling induced breakup, and rebound with break up were discussed in detail. Results showed that the solute has a strong effect on the outcome of droplet impingement promoting droplet disintegration and enhance bubble formation. Wang et.al., [28] conducted experiments on droplet impact on the preheated polished and rough surfaces of silicon carbide and stainless steel. The effects of impact behavior, contact angle surface roughness, and thermal properties are discussed in detail heat transfer. The experiments are carried out in the range of 10 <We<120 and $T_{surf} < 460°C$. Simhadri Rajesh et.al., [29] performed experiments to explain the thermo-hydrodynamic behavior of droplet impingement on superheated cylindrical surfaces. The surfaces have concave and convex profiles that offer asymmetric zone for droplets to expand and retract. The water droplet was used to carry out experiments to visualize droplet evolution by having Weber numbers varied between 5 to 65 and surface temperature ranged from 125°C to 290°C. Ma et.al., [30] experimentally examined single deionized water droplet on superheated aluminum plates having a very small roughness. During work six typical droplet impact and boiling modes were observed and classified into Ts-We regime map. It was also found that surface wettability has significant effect on Ts-We regime map. It was observed that droplet rebound required higher surface temperature for hydrophilic surface and in case of lower surface temperature droplet breakup is not observed. In [31] Illias et.al., experimentally and numerically examined the spreading phenomena of a water droplet in the film boiling region. During the work, it was found that in film boiling region, variation in surface temperature does not affect the droplet spreading. Misyura [32] experimentally investigated the evaporation of water and aqueous salt solution droplets. The effects of vapor-gas convection on droplet evaporation were studied thoroughly and found that neglecting of gas convection leads to underestimation of the evaporation rates. In [33] Gholijani et.al., carried out experiments to study the influence of the drop

impact diameter, drop impact velocity and wall superheated on hydrodynamics and heat transport of droplet impacting on heated wall. The drops used for this study was FC-72 in a pure vapor atmosphere. During study it was found that, larger drop diameters, higher impact velocities and higher wall superheats results in increasing heat flow after the impact. It was also found that maximum spread is inversely proportional to wall superheat and directly proportional to impact diameter and rising impact velocity. Cetiner et.al., [34] experimentally investigated the droplet impact on different surface topographies. In order to prevent the liquid attachment at the wall major work is devoted in developing of super hydrophobic surface. Effect of deionized water droplet impact on five different surface i-e, polished, laser-ablation, anodization, super hydrophobic spray-coated was observed. The experiments were carried out to study the effects of surface temperature and velocity on spread dynamics. Pan.et al., [35] developed a comprehensive model to predict the sessile droplet evolution and local evaporation flux on heated super hydrophobic, hydrophobic and hydrophilic substrates. Dinc and Gray [36] numerically examined the effect of gravity and drop shape of impinging water droplets on the wet, flat and isothermal surface. 2D-axisymmetric simulations were performed using ANSYS fluent for different gravity conditions keeping fixed Re = 6690, We = 139, $\frac{h}{D} = 0.837$, contact angle= $0^o$. In Xu et.al., [37] numerically examined the drop impacting on a uniformly hydrophilic, hydrophobic, and surface heterogeneous surface. During the studied it was found that capillary wave enhances drop breakup mechanism. Transition boundaries between drop breakup and non-breakup were given over a wide range of We, Oh, and Bi numbers. In order to develop a correlation for the maximum generated pressure Marzbali and Dolatabadi [38] studied the effects of droplet size, impingement velocity, and liquid film thickness. Aim of this study was to develop a correlation for generated pressure during high speed droplet impact. Tian and Chen [39] experimentally examined the impingement of non-evaporating droplets of four liquids, that is, R113, ethanol, deionized water, and acetone. The impact velocity, droplet diameter, viscosity, and surface tension were considered important investigation parameters Results illustrated that the large surface tension and viscosity hindered the droplet spreading whereas droplet diameter has minimal effect.

Despite the previous rigorous efforts the investigation of evaporation dynamics of drop-wall collision, more researches are require on drop parameters (drop diameter, impact velocity), physical properties (saturation temperature, density, viscosity, and surface tension), surrounding gas parameters (pressure, temperature, properties, velocity, and flow configuration) and wall characteristics (wettability, diffusivity, surface roughness, and wall temperature). The main novelty of this research work is to numerically investigate the effect of thermal boundary layer, drop size and drop velocity impact on evaporation dynamics of drop-wall collision. We select droplet diameter 0.925 mm to 1.6 mm, drop velocity 0.325 to 0.576 based on the experimental work of Gholijani et.al., [33].

# Chapter 3

# Mathematical Modeling

## 3.1 Volume of Fluid

To solve the two-phase flow of liquid droplets inside a vapor medium, the Volume of Fluid Method (VOF) is employed. Volume of fluid (VOF) method is used to capture the pattern of liquid and vapor phase by solving equations of the volume fraction,$\alpha$. The volume fraction of each cell lies between 0 and 1. If the volume fraction of liquid is zero in grid cell then the whole cell is occupied by vapor phase. If the liquid volume fraction is unity in grid cell then the cell is fully occupied by liquid phase. Otherwise, in each cell of the grid, sum of the liquid and vapor fraction always be unity as shown in equation 3.1.

$$\alpha_l + \alpha_v = 1 \tag{3.1}$$

The governing equations for the liquid and vapor volume fractions is equation 3.2 and 3.3

$$\frac{\partial \alpha_l}{\partial t} + \nabla.(\vec{v}\alpha_l) = \frac{\dot{m}_l}{\rho_l} \tag{3.2}$$

$$\frac{\partial \alpha_v}{\partial t} + \nabla.(\vec{v}\alpha_v) = \frac{\dot{m}_v}{\rho_v} \tag{3.3}$$

Whereas, mass dissipated by liquid phase is equal to the mass gain by vapor phase, $\dot{m}_l + \dot{m}_v = 0$. So, no equation is solved for the gas volume fraction, as the values of $\alpha_v$ are calculated from the $\alpha_l$ according to equation 3.1. For the

solution, volume fraction equation is coupled with the continuity and momentum conservation equations and can be expressed as

$$\frac{\partial \rho}{\partial t} + \nabla.(\rho \vec{v}) = 0 \tag{3.4}$$

$$\frac{\partial}{\partial t}(\rho \vec{v}) + \nabla.(\rho \vec{v}\vec{v}) = -\nabla p + \nabla.[\mu(\nabla \vec{v} + \vec{v}^T)] + \rho \vec{g} + F_v \tag{3.5}$$

In comparison to other techniques, VOF model is solved for both liquid and vapor phase. Material properties such as density and viscosity are updated according to the value of volume fraction in each cell as a function of liquid volume fraction using linear interpolation between the values of the two phases as shown in equation 3.6 and 3.7

$$\rho = \rho_l \alpha_l + (1 - \alpha_l)\rho_v \tag{3.6}$$

$$\mu = \mu_l \alpha_l + (1 - \alpha_l)\mu_v \tag{3.7}$$

In equation 3.5 $F_v$ is the volume force due to surface tension. The Brackbill Continuum Surface Force (CSF) [40] model describe the relationship between the volume force and the surface tension force as described in equation 3.8.

$$F_v = \sigma \frac{\alpha_l \rho_l \kappa_l \nabla \alpha_l + \alpha_v \rho_v \kappa_v \nabla \alpha_v}{0.5(\rho_l + \rho_v)} \tag{3.8}$$

Where is $\kappa$ the interface curvature is obtained from

$$\kappa_l = -\kappa_v = -\nabla.(\frac{\nabla \alpha_l}{|\nabla \alpha_l|}) \tag{3.9}$$

Whereas, $\nabla \alpha_l$ represent the change in volume fraction in grid cell.

## 3.2 Phase Change Model

In order to account for the evaporation of liquid droplet, an additional energy equation is solved with the Volume of fluid model.

$$\frac{\partial}{\partial t}(\rho h) + \nabla.(\rho \vec{v} h) = \nabla.(K \nabla T) + S_h \tag{3.10}$$

whereas, $h$ and $K$ represents the enthalphy and thermal conductivity for mixed phase.

$$h = \frac{\alpha_l \rho_l h_l + \alpha_v \rho_v h_v}{\alpha_l \rho_l + \alpha_v \rho_v} \tag{3.11}$$

$$K = K_l \alpha_l + (1 - \alpha_l) K_v \tag{3.12}$$

In 1980 [41], Lee proposed the simplified saturation phase change model that is widely used for the study of evaporation and condensation process, where the liquid and vapour mass transfer process is controlled by the vapor transfer equation:

$$\frac{\partial \alpha_v \rho_v}{\partial t} + \nabla.(\alpha_v \rho_v \vec{v}) = \dot{m}_{lv} - \dot{m}_{vl} \tag{3.13}$$

Mass transfer model can be described based on temperature difference. When the temperature of liquid phase is greater then the saturation temperature then mass is transferred from liquid phase to vapor phase. On the other hand if temperature of vapor phase is less then the saturation then mass is transferred from vapor to liquid phase and condensation phenomena occurs. This phenomena is also expressed in equation 3.14 and 3.14

If $T_l > T_{sat}$ (evaporation):

$$\dot{m}_{lv} = Coeff \times \alpha_l \rho_l \frac{T_l - T_{sat}}{T_{sat}} \tag{3.14}$$

If $T_v < T_{sat}$ (condensation):

$$\dot{m}_{vl} = Coeff \times \alpha_v \rho_v \frac{T_{sat} - T_v}{T_{sat}} \tag{3.15}$$

Where Coeff is mass transfer intensity factor with unit $s^{-1}$. "Coeff" is a key value when investigating droplet evaporation and it is to be such a value that avoids divergence issues and maintain the interfacial temperature close to the saturation temperature. As an empirical coefficient, Coeff is given different values for different problems. To identify the specific Coeff of the mass transfer model numerous simulations need to be conducted for to tune results related to experiment. Value of empirical constant Coeff can be upto $5 \times 10^6$ as mentioned in [42]. In drop-drop evaporation selected "Coeff" is 10000 to keep the droplet temperature near to saturation temperature. Whereas, for drop-wall interaction the chosen value of

"Coeff" is 0.1 to tune it according to experimental results.

## 3.3 Wettability

An ability of liquid to maintain contact with rigid body is known as wettability. The effect of wall adhesion/wettabililty can be easily estimated within the framework of continuum surface model. Rather than to impose this as boundary condition at the wall, the contact angle that the fluid is assumed to make with the wall is used to adjust the surface normal in cells near the wall. Implemented contact angle may be static or dynamic.[42]

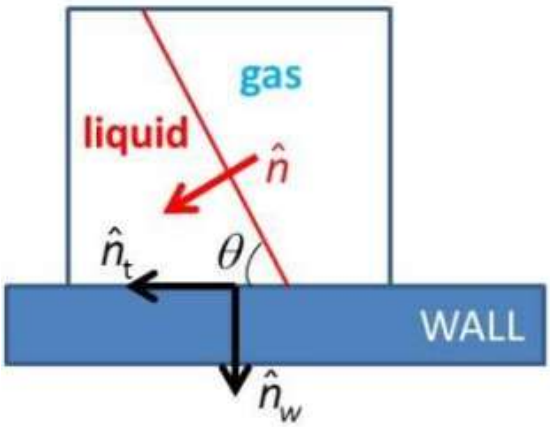


FIGURE 3.1: Unit vectors on the wall face, as well as unit free surface normal vector [42]

Based on the contact angle value $\theta$, which should be prescribed, the normal to the interface unit vector at the wall boundary cells $\hat{n}$ is calculated according to the following equation:

$$\hat{n} = \hat{n}_w cos\theta_n + \hat{n}_t sin\theta_w \tag{3.16}$$

where $\hat{n}_w$ and $\hat{n}_t$ are the unit vectors normal and tangent to the wall. The combination of this contact angle with the normally calculated surface normal one cell away from the wall determine the local curvature of the surface, and this curvature is used to adjust the body force term in the surface tension calculation. Figure 3.1 is presented for better understanding of equation 3.15 concept and notation.

# Chapter 4

# Evaporation Dynamics during Drop-Drop Interaction in Vapor Medium

This chapter provides the setup and results details of the numerical modeling of drop-drop interaction in single vapor medium. The numerical model is first validated with the numerical results available in the literature. Following that, two interacting droplets in inline and lateral configurations are investigated by varying spacing between two droplets. Additionally, in inline configuration, two arrangement patterns: big-small arrangement (BSA) and the small-big arrangement (SBA), are investigated. Normalized $d^2$, is the representation of the time evolution of the droplet evaporation. This study enables us to understand the effect of arrangement pattern, droplet initial distance ratio and droplet size ratio affect on the evaporation dynamics of droplets.

## 4.1 Numerical Solution Strategy

The governing equations for the evaporation of the moving droplet are numerically solved in the 2D planar domain using the commercial CFD package ANSYS Fluent 2020 R2. A pressure-based-segregated code and Pressure Implicit with Splitting

of Operator (PISO) algorithm is used to solve continuity and momentum equations. During the calculation, a Quadratic Upstream Interpolation for Convective Kinematics (QUICK) scheme is employed for spatial discretization of the energy and momentum equation. To discretize the pressure equation Pressure Staggering Option) PRESTO scheme is used. For transient formulation, a first-order implicit scheme is used. Volume fraction equations with explicit formulation are solved by using the Geo-Reconstruct scheme.The Geo-Reconstruct scheme used piecewise-linear approach to represents the interface between two fluids. Relaxation factors used for pressure and momentum equation are 0.3 and 0.7, while for body forces and energy equation relaxation factor used is 1. Convergence criteria $10\times10^{-6}$ are used for the accuracy and stability of the solution.

## 4.2 Important Non-Dimensional Numbers

The important dimensionless numbers are summarized below: **Eötvös number (Eo)** is a ratio of gravitational and surface tension forces and it is used to characterize the shape of drops moving in a surrounding fluid.

$$Eo = \frac{(\rho_l - \rho_g)d^2 g}{\sigma} \tag{4.1}$$

**Morton number (Mo)** is used together with the Eötvös number to specify the shape of the moving droplet.

$$Mo = \frac{\mu_g^4(\rho_l - \rho_g)g}{\rho_g^2\sigma^3} \tag{4.2}$$

The **Stefan number (St)** is defined as the ratio of sensible heat to latent heat.

$$St = \frac{C_{p,g}(T_\infty - T_{sat})}{h_{lg}} \tag{4.3}$$

**Density ratio ($\eta$)**is the ratio of the density of liquid $\rho_l$ and density of gas $\rho_g$.

$$\eta = \frac{\rho_l}{\rho_g} \tag{4.4}$$

**Viscosity ratio ($\lambda$)** is the ratio of the viscosity of a liquid $\mu_l$ and viscosity of gas $\mu_g$ phase.

$$\lambda = \frac{\mu_l}{\mu_g} \tag{4.5}$$

**Prandtl number (Pr)** measure momentum diffusivity compared to thermal diffusivity.

$$Pr = \frac{\mu C_p}{K} \tag{4.6}$$

**Initial distance ratio ($S_x$)** is the ratio of the distance $L_x$ between the centroid of lateral drops and characteristic radius $r_o$ of a droplet.

$$S_x = \frac{L_x}{r_o} \tag{4.7}$$

**Initial distance ratio ($S_y$)** is the ratio of the distance $L_y$ between the centroid of lateral drops and characteristic radius $r_o$ of a droplet.

$$S_y = \frac{L_y}{r_o} \tag{4.8}$$

**Size ratio (R)** is the ratio of smaller drop radius $r_s$ and characteristic radius $r_0$ of a droplet.

$$R = \frac{r_s}{r_o} \tag{4.9}$$

**Normalized $d^2$** is the ratio of evaporating drop diameter to droplet initial diameter

$$Normalized\ d^2 = (\frac{d}{d_o})^2 \tag{4.10}$$

Where, the equation of **overall normalized $d^2$** is

$$Overall\ (\frac{d}{d_o})^2 = \frac{\sum d^2}{\sum\ d_0^2} \tag{4.11}$$

The **non-dimensional time, $\tau$** is represented by

$$\tau = \sqrt{\frac{d_o}{g}} \tag{4.12}$$

whereas, $d_0$ is the inital drop diameter and g represents the gravitational acceleration.

## 4.3 Verification and Validation

### 4.3.1 Evaporation of Single Moving Droplet

The computational domain used for the validation of two-dimensional single moving droplet is depicted in Figure 4.1. Droplet with initial diameter $d_0 = 0.25$ mm is centered at $x_c$=0.5 mm from left wall and $y_c$=3.6 mm from the bottom wall in a numerical domain of $1 \times 4$ mm$^2$. The temperature value of the droplet stays fixed at saturation value throughout the simulation, i.e., $T_{sat}$=373 K . Boundaries of the domain are specified as walls and wall temperature is fixed at $T_{wall}$=480 K. The physical properties are selected to have the non-dimensional parameters as Mo $= 10 \times 10^{-4}$, Eo $= 10$, St $= 0.1$, $Pr_l$= 5.37, $Pr_v$= 1.0, $\eta$= 5 and $\lambda$= 20. The time scale for mentioned case is $\sqrt{\frac{d_0}{g}}$ and the length scale is equal to initial droplet diameter $d_0$.

For validation of our numerical methodology adopted in this study, results are

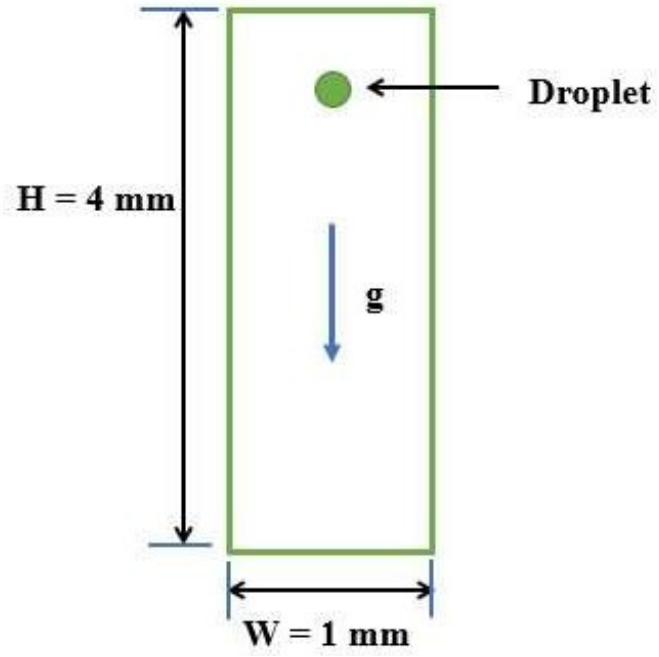


FIGURE 4.1: Computational domain for validation of single moving droplet

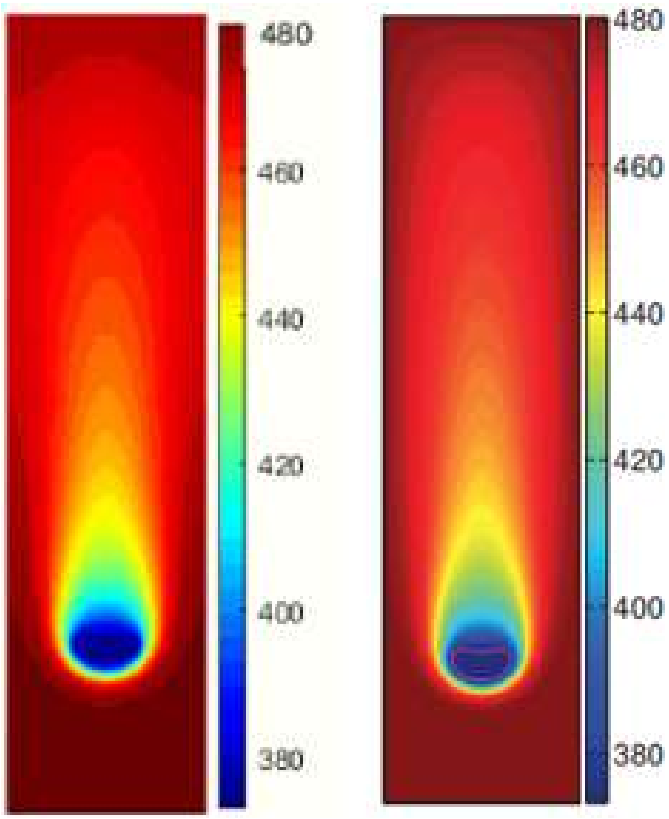


FIGURE 4.2: Comparison of Temperature contours for single moving droplet: Present simulation (left) and Irfan and Muradoglu [10](Right)

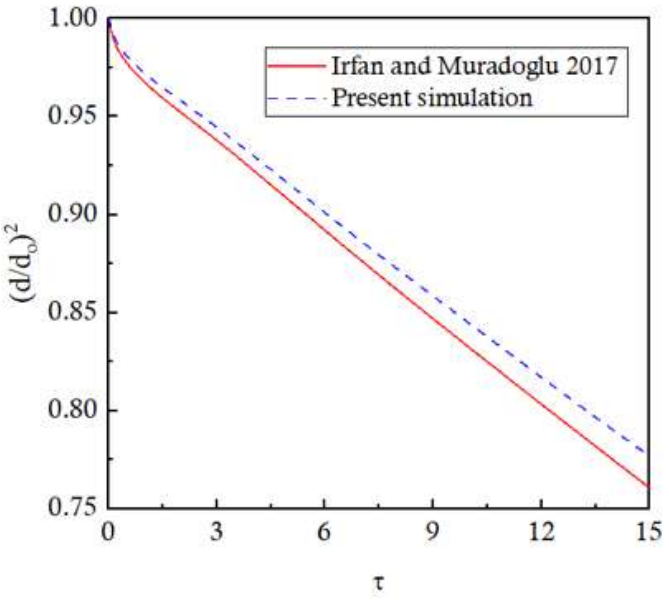


FIGURE 4.3: Comparison of evolution of the Normalized $d^2$ between present simulation and Irfan and Muradoglu [10]

compared to those in the literature. Numerical results of Irfan and Muradoglu [10] when compared to the current methodology are approximately equal. Results

of the temperature contour and normalized $d^2$ as shown in Figure: 4.2 and 4.3. The result of normalized $d^2$ is provided by Irfan and Muradoglu [10] on request. They used Front tracking code in combination with temperature gradient based evaporation model.

### 4.3.2 Evaporation of Two ln-line and Lateral Moving Droplets

The computational domain used for the validation and numerical study of two in-line and lateral drops moving in Cartesian coordinates is shown in Figure 4.4 and 4.5.

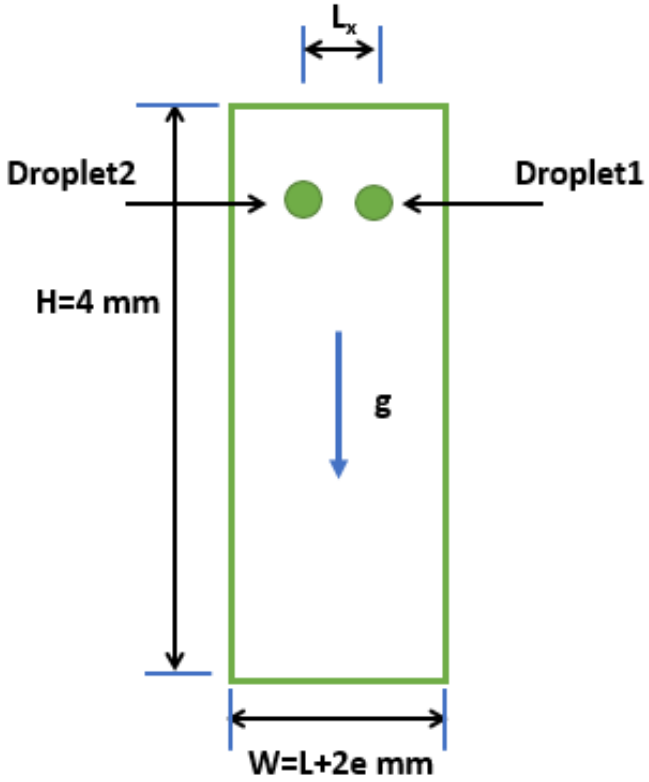


FIGURE 4.4: Computational domain for validation and numerical study of lateral drops

In lateral case, distance between the centroid of two droplets is varied by initial distance ratio $S_x$ and accordingly, the width of the fluid domain is varied, keeping height fixed at 4 mm.

Similarly, for the inline case, centroid of droplet 1 (leading droplet) is 3 mm far from the bottom wall and the droplet 2 centroid (trailing droplet) has a fixed

distance from the bottom wall is (3+$L_y$) mm. In inline case fluid domain has a fixed width of 2 mm and height is varied according to the initial distance ratio $S_y$.

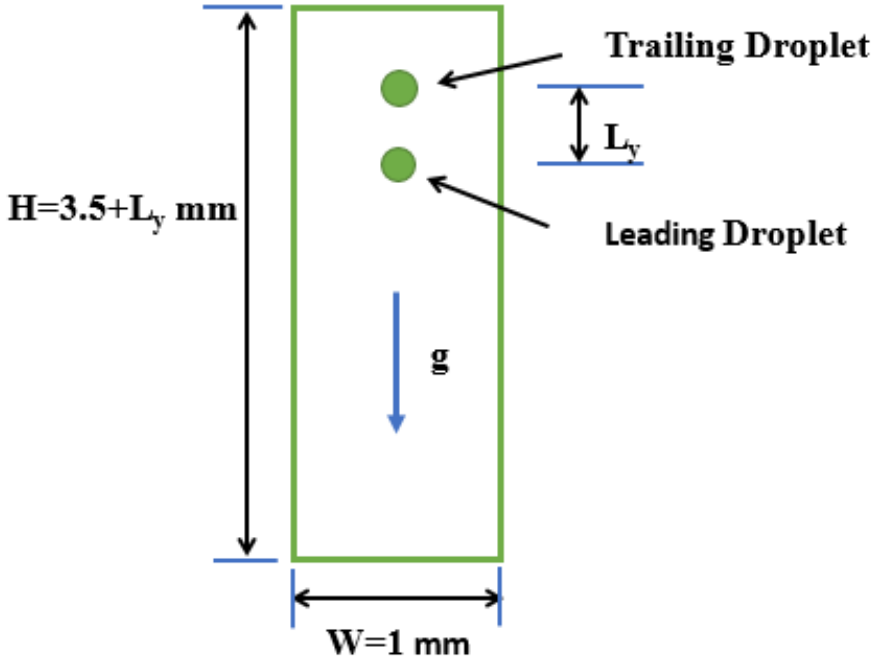


FIGURE 4.5: Computational domain for validation and numerical study of Inline drops

For validation of our numerical methodology adopted in this study, results are compared with the Front tracking code of Irfan and Muradoglu [10] and a good agreement is observed between the two results. For lateral configuration, the normalized $d^2$ and droplet trajectory are compared as shown in Figure 4.6 and for inline arrangement normalized $d^2$ and droplet y location is compared as shown in Figure 4.7. The physical properties are selected to have the non-dimensional parameters as Eo = 5, Mo = $5 \times 10^{-4}$, St = 0.1, Sc = 1, $Pr_l$ = 5.37, $Pr_g$ = 1.0, $\eta$= 5 and $\lambda$ = 20.

### 4.3.3 Grid and Time-Step Independence

To avoid numerical errors in the computational results, grid convergence studies are performed for both inline and lateral configuration. Three different types of a

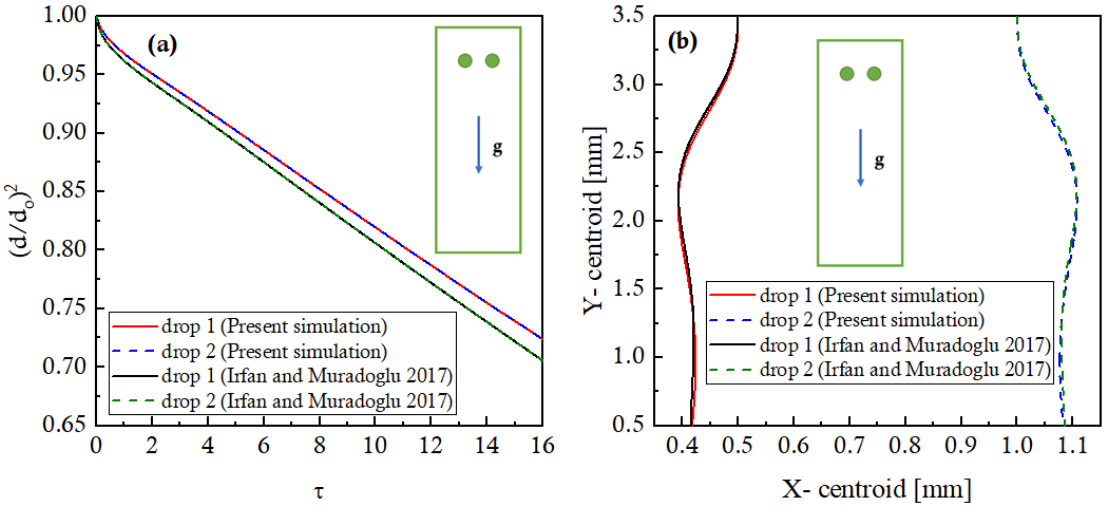


FIGURE 4.6: Results comparison for lateral configuration: (a) represents normalized $d^2$ and (b) represents droplet trajectory

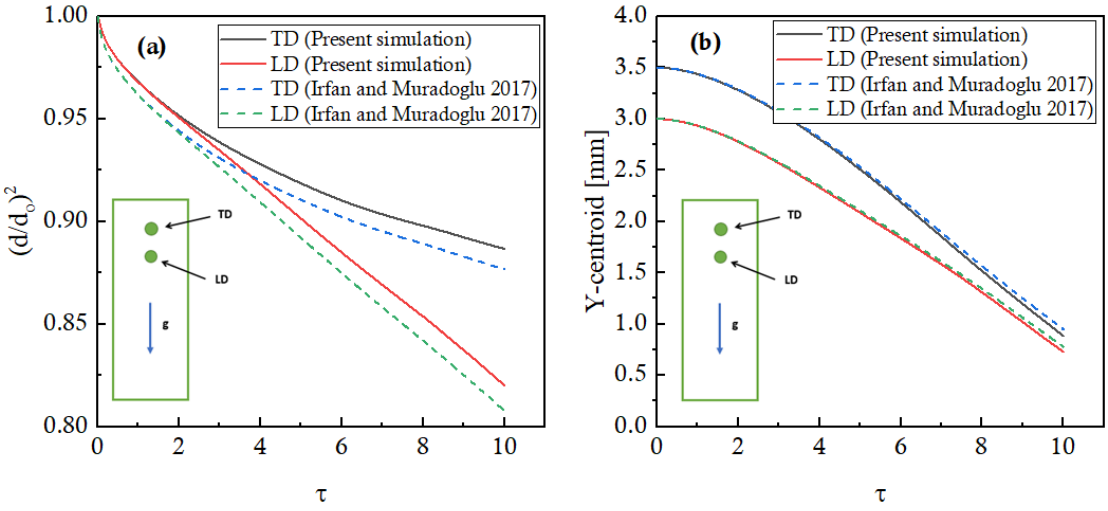


FIGURE 4.7: Results comparison for inline configuration: (a) represents normalized $d^2$ and (b) represents droplet Y-centroid

structured grid is selected on the base of edge sizing for grid 1 1mm is divided into 32 division. Similarly, for grid 2 and grid 3, 1 mm is divided into 64 and 128 divisions,respectively. For lateral configuration Grid 1, Grid 2, and Grid 3, consisting of (48×128), (96×256), and (192×512) computational cells are investigated for the domain of 1.5×4 mm$^2$. Comparably, For inline configuration Grid 1, Grid 2, and Grid 3, consisting of (32×128), (64×256), and (128×512) computational cells are investigated for the domain of 1×4 mm$^2$.

For lateral configuration, simulation is run for all three grids, the temporal evolution of the area ratio is plotted shown in Figure 4.8 (a). At $\tau$=18 the maximum

difference between normalized $d^2$ results for Grid 1 and Grid 3 is under 1.5 % while, for Grid 2 and Grid 3, this difference reaches 0.12%. Therefore, Grid 2 is chosen for the current study. Similarly, to study grid convergence for inline configuration simulation is run before the coalescences between drops occur. For all three grids, the temporal evolution of the area ratio is plotted shown in Figure 4.8 (b). At $\tau$=10 the maximum difference between normalized $d^2$ results for Grid 1 and Grid 3 is under 1.5% while, for Grid 2 and Grid 3, this difference reaches 0.12%. Therefore, Grid 2 is selected for the current study.

To investigate the time-step size effects on the solution, comparisons of the

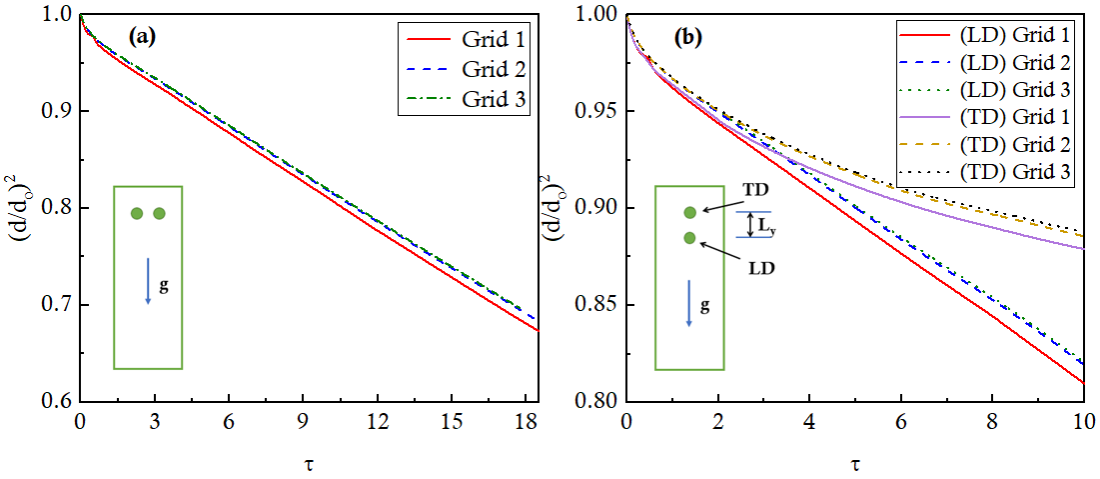


FIGURE 4.8: Normalized $d^2$ results comparison for different grid resolution (a) for lateral configuration and (b) for inline configuration

courant number 0.1 and 0.25 are performed for both inline and lateral configuration as shown in Figure 4.9 (a) and (b). With the current methodology, courant number 0.25 keeps the solution stable and accurate.

## 4.4 Results and Discussion

In this section the results of the simulations for drop-drop interaction will be presented. First, the simulation is performed to investigate the effect of initial distance ratio $S$ on droplet evolution for both inline and lateral configuration. Afterwards the effect of size ratio $R$ for small-big arrangement is monitored. Finally, the effect of arrangement pattern on droplet interaction is studied. In this

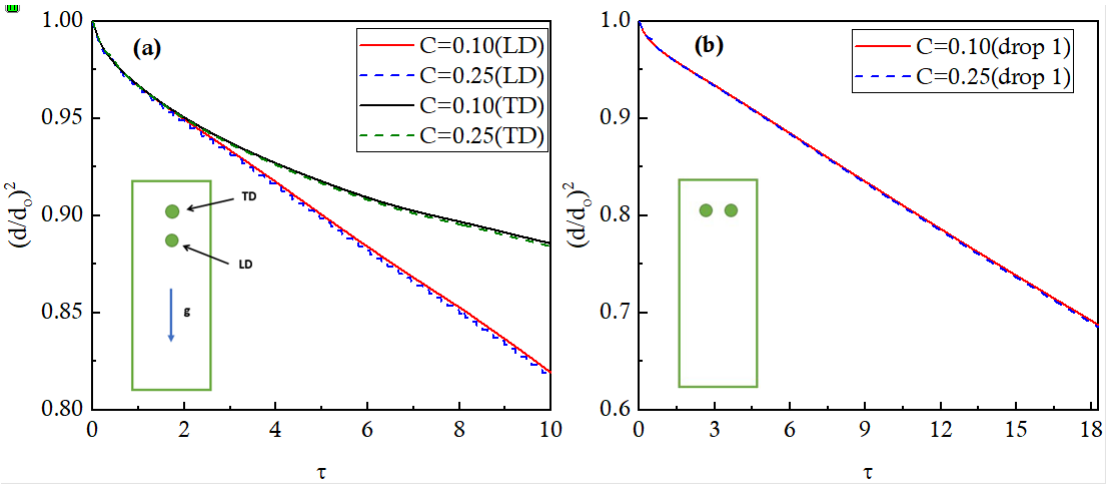


FIGURE 4.9: Normalized $d^2$ results comparison for courant 0.1 and 0.25 (a) for lateral configuration and (b) for inline configuration

study normalized $d^2$, droplet velocity and distance between droplets are considered important parameters.

### 4.4.1 Effect of Initial Distance Ratio, S

The effect of the initial distance ratio on evaporation and coalescence is studied using the initial distance ratio $S_x$ and $S_y$ from 4 to 12 for both lateral and inline configuration while keeping R constant as 1. In the lateral configuration, droplet 1 and droplet 2 are centered at (e mm, 3.5 mm) and (e+$L_x$ mm, 3.5 mm), where e represents the distance between drop centroid and its side wall. For inline configuration, droplet 1 is the leading droplet which starts from a fixed position (0.5 mm, 3mm) and droplet 2 is trailing droplet which is initially positioned at (0.5 mm,3+$L_y$ mm). The value of $L_x$ and $L_y$ is increased by increasing $S_x$ and $S_y$. Normalized $d^2$ which is an indicator of evaporation rate and droplet velocities considered as important parameters and continuously monitored.

Figure 4.10 (a) and (b) represent the influence of initial distance ratio on evolution of normalized $d^2$ for leading and trailing droplet respectively. Two main points are observed from Figure 4.10 (a) and (b). First observation is that by varying $S_y$ in inline arrangement negligible effect on normalized $d^2$ notice for the case of the leading droplet that can be ignored. Whereas, for trailing droplet simulation

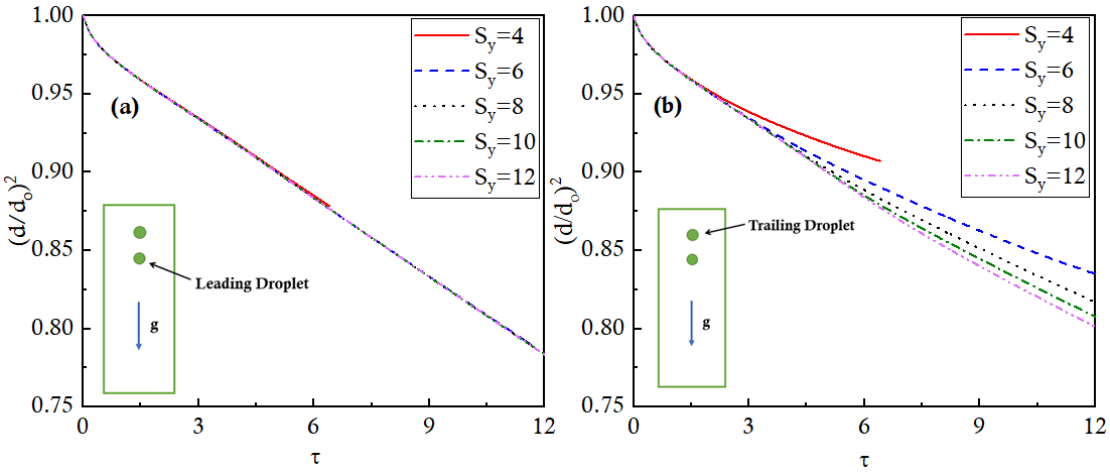


FIGURE 4.10: Influence of initial distance ratio $S_y$ on the normalized $d^2$ (a) for leading droplet (b) for trailing droplet

results shows that increase in $S_y$ results in increase the droplet evaporation. Second point is noticed that for fixed initial distance ratio leading drop evaporates faster as compares to trailing droplet.

Contour plots of droplet temperature for the inline configuration at time $\tau$ = 3 and 9 are shown in Figure 4.11. Rows correspond to different spacing ratio whereas the columns represent different times during the evaporation. For fixed $S_y$ the leading droplet evaporates faster because its front is moving through high-temperature vapor. In its trace trailing droplet front find an area with vapor at significantly lower temperature compared with the temperature at the front of the leading droplet. The trailing droplet while passing through this vapor area is heated up to a quite lower temperature than the leading droplet. Similarly by increasing initial distance ratio $S_y$, the gap between leading and trailing droplet increases. So,with an increase in $S_y$ the trailing droplet find high temperature gas area infront of it. With increase in $S_y$ the trailing droplet is heated more and leads to faster evaporation. Figure 4.12 represents the overall evolution of droplets for different initial distance ratio. It can be seen that increase in $S_y$ reduce the time required for droplet evaporation.

Figure: 4.13 represents the velocity vectors of inline configuration for time $\tau$=0.5, 2.5, 4.5 and 6.5. It is noticed that smaller the initial distance between consecutive droplets, the more intensive is the process of their approach and of the next union. Intensification in evaporation of leading droplet as compared to

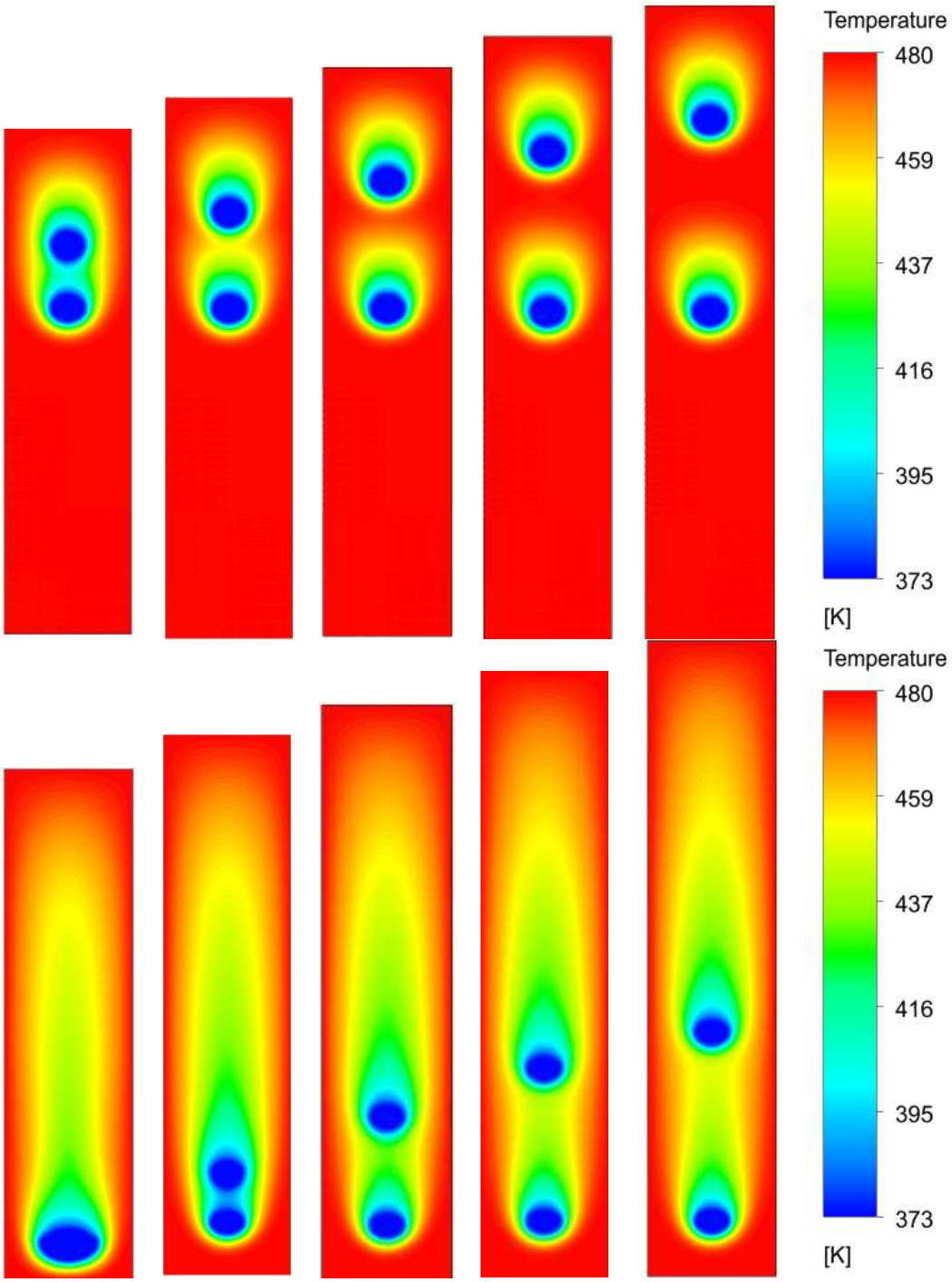


FIGURE 4.11: Contour plots of Temperature (top row) at fixed time $\tau$ =3, and (bottom row) at fixed time $\tau$ =12, showing the evolution of an evaporating droplet (from left to right) at spacing 4,6,8,10 and 12

trailing droplet leads to increase in velocity of trailing droplet as compared to the leading one. Moreover, one can find that in Figure 4.14 (a) and (b) for case $S_y$=4 coalescence of droplets occur early as compare to $S_y$=5.

Figure 4.15 show the influence of initial distance ratio on the velocity of leading

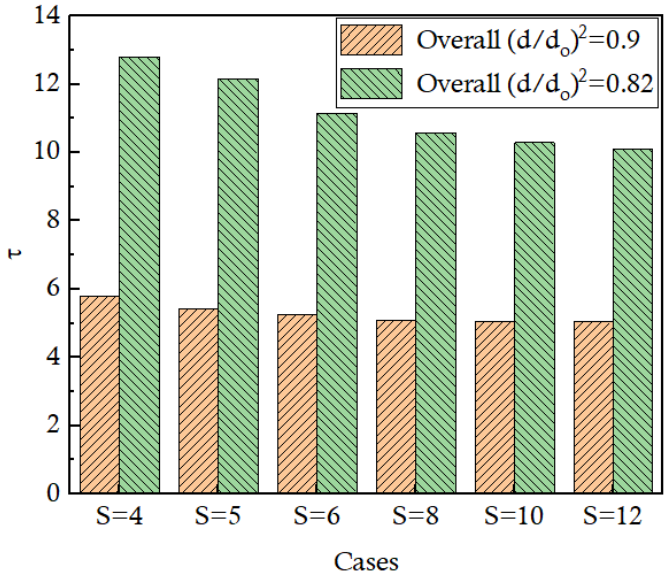


FIGURE 4.12: Influence of initial distance ratio on the overall normalized $d^2$ for inline configuration

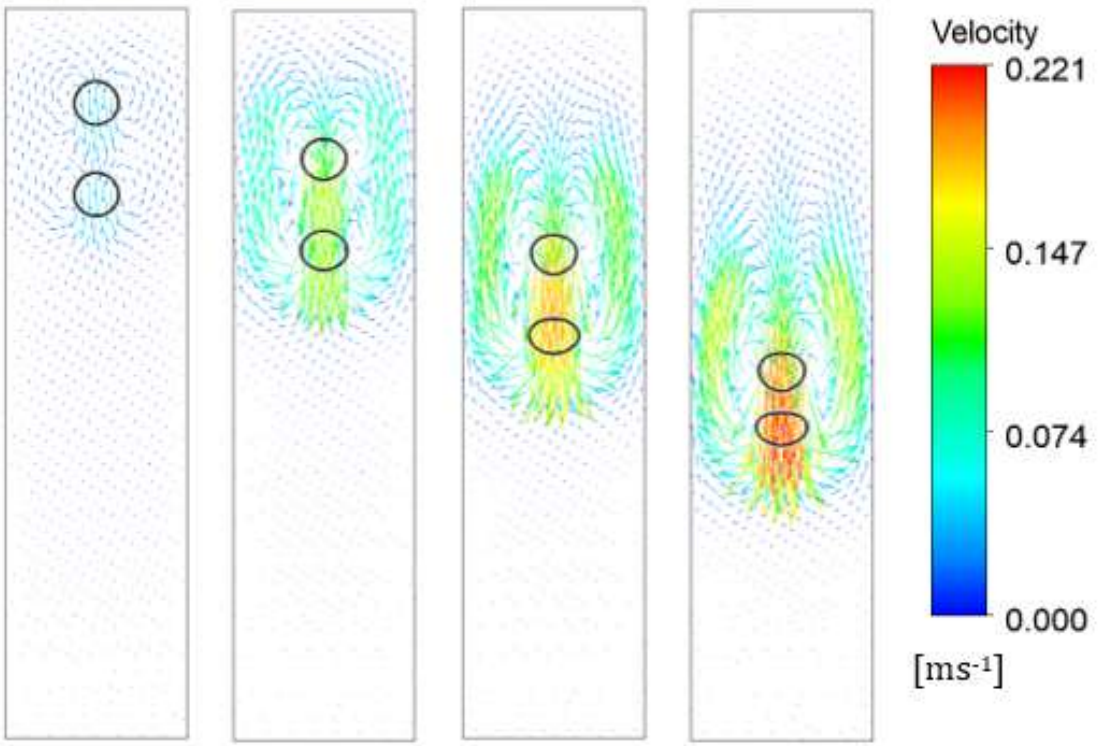


FIGURE 4.13: Velocity vectors of an evaporating droplet for fixed initial $S_y$ =4 (from left to right) at $\tau$ = 0.5,2.5,4.5,and,6.5

droplet and trailing droplet.It is observed that the velocities of the two droplets were identical in the first part of their trajectories for time $\tau = 1.2$. This is due to the thermal inertia of droplets. The velocity of the trailing droplet is largely

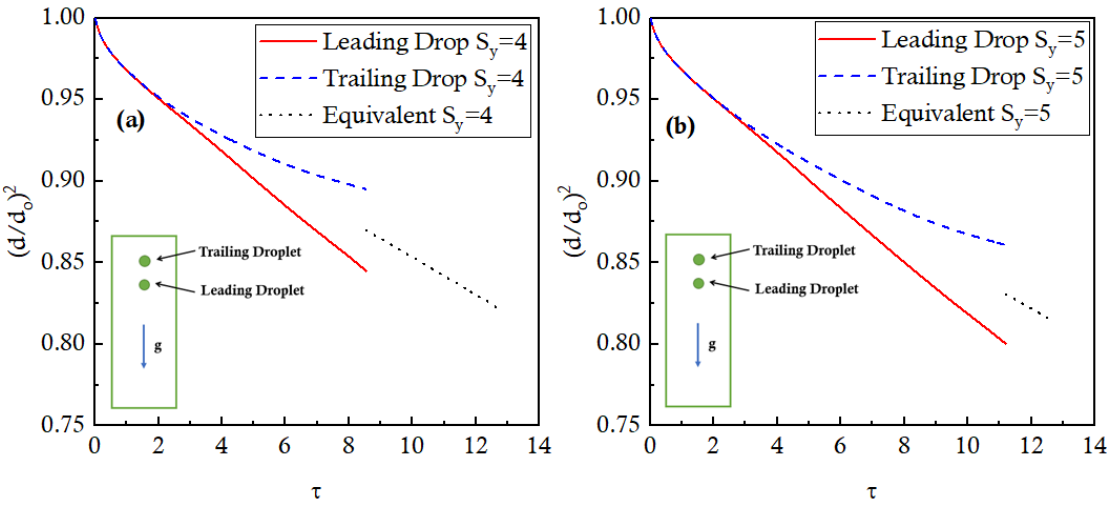


FIGURE 4.14: Influence of initial distance ratio on the normalized $d^2$ (a) for $S_y$ =4 and (b) for $S_y$ =5

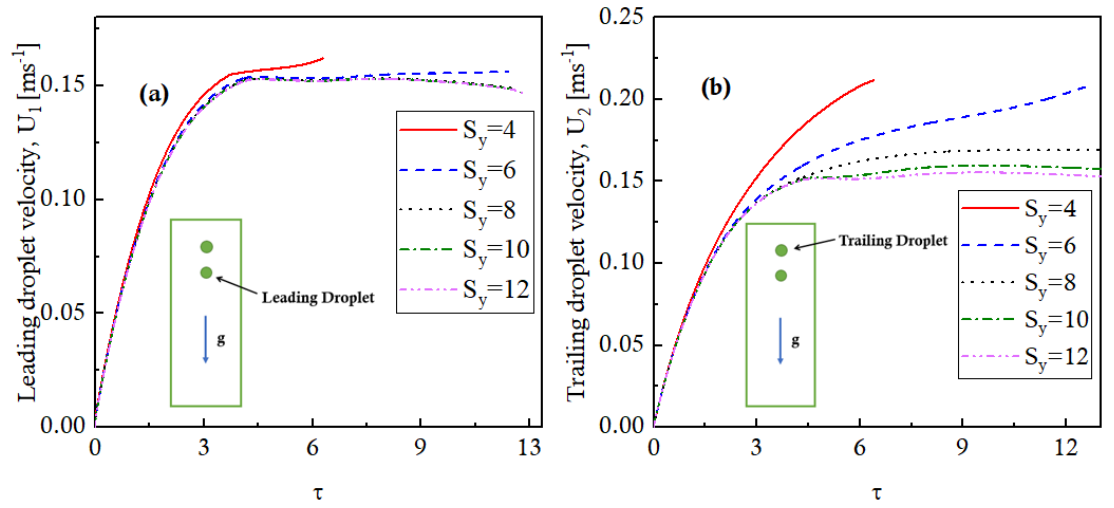


FIGURE 4.15: Influence of initial distance ratio on the droplet velocity (a) leading droplet and (b) for trailing droplet

influenced by the presence of a leading droplet. The evaporation of the leading droplet forms a buffer layer as part of a thermal protection at its back end. It creates the conditions for decreasing the heat-up rates and the evaporation of successive droplet. Increase in initial distance ratio reduced the effect of buffer layer on trailing droplet that leads to higher evaporation rate and decreased acceleration of leading droplet.

For lateral configuration, first a domain independence study is carried out by varying distance from drop centroid to its side wall (e) from $2d_o$ to $14d_o$ and keeping fixed initial distance ratio $S_x$=4. From study it is found that evolution of

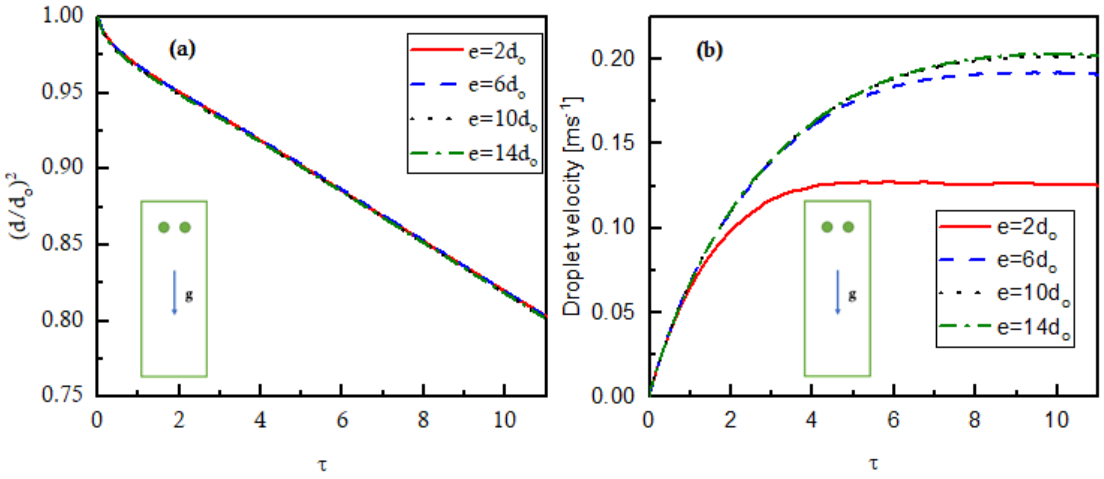


FIGURE 4.16: Influence of drop to wall distance in lateral configuration by keeping $S_x$=4 (a) normalized $d^2$ (b) droplet centroid velocity

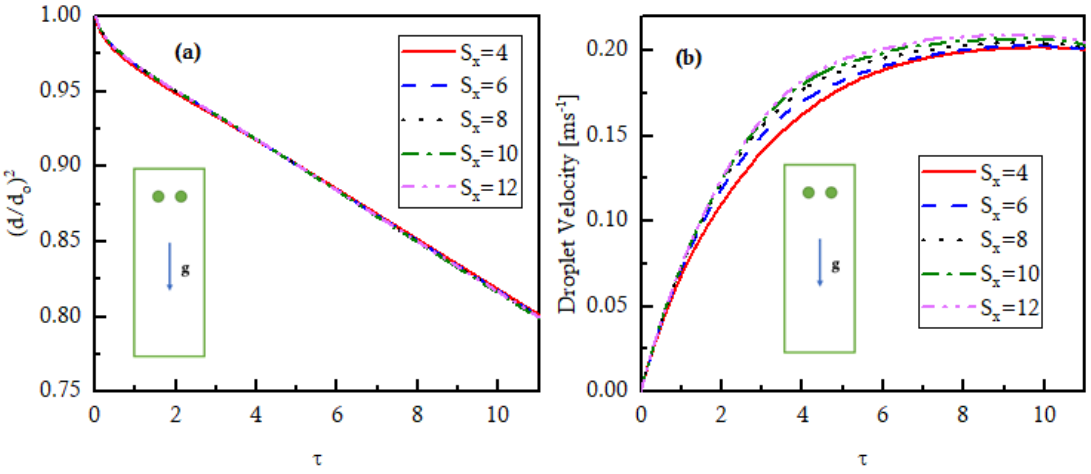


FIGURE 4.17: Influence of initial distance ratio $S_x$ in lateral configuration (a) normalized $d^2$ (b) droplet centroid velocity

drop is independent of "e" as shown in Figure 4.16 (a), where no effect on drop velocity is observed when the the distance of drop centroid to its side wall is grater or equal to $10d_o$ as shown in Figure 4.16 (b). In the lateral configuration when the initial distance ratio $S_x$ increase it has a negligible effect on normalized $d^2$ as depicted in Figure 4.17 but a major effect on drop velocity is noticed. In lateral configuration droplet 1 and droplet 2 are symmetric. It is observed that due to thermal inertia of droplets the velocities of the two droplets were identical in the first part of their trajectories for time $\tau$=1.2. As droplets start to move, a buffer layer is formed between droplet 1 and 2. The droplets facing buffer area evaporate slow as compared to other faces due to which the center-of-mass of the droplet also

oscillates or deviates from its original location and decrease its velocity towards the bottom wall. With increase in $S_x$ effect of buffer layer getting minimal that also minimize the deviation of droplet from its original path and leads to increase in velocity towards the bottom wall.

### 4.4.2 Effect of Size Ratio

Inline configuration is selected to study the effect of size ratio on the evaporation and coalescence of the leading and the trailing droplets. We compare size ratio R from 0.5 to 0.9 for small-big arrangement (SBA). Droplets start to move due to gravity after they are released. Normalized $d^2$, droplet velocities, and distances between them are considered as important and continuously plotted. For the SBA case at R = 0.5 to 0.9, the normalized $d^2$ is plotted in Figure 4.18 (a) and (b) for both leading and trailing drops. It is observed that in SBA when the sizing ratio decrease from 0.9 to 0.5, leading drop has a negligible effect on evaporation. On the contrary an increasing trend is observed for evaporation of trailing droplet.

Increase in evaporation rate for R=0.5 as compared to R= 0.9 is strengthened

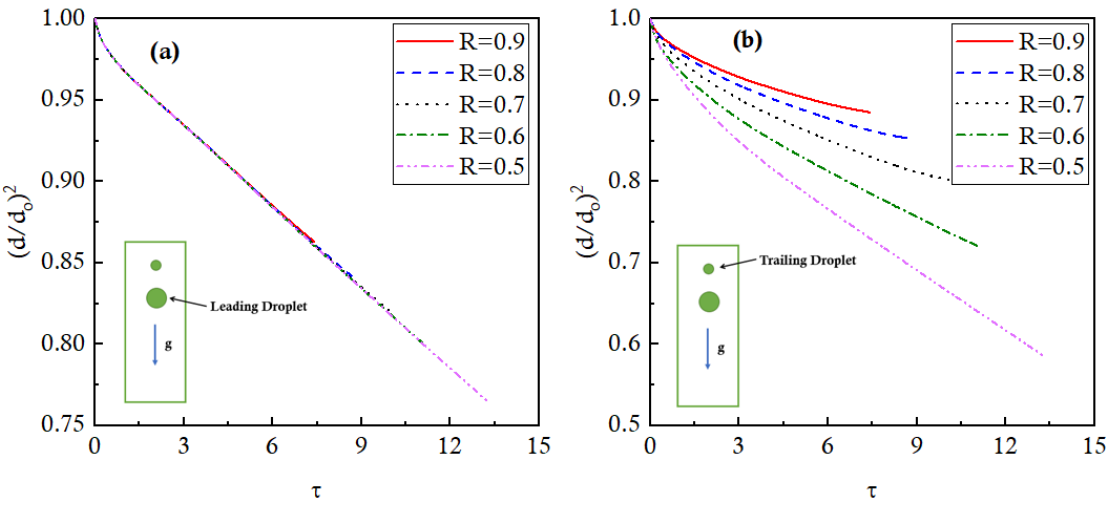


FIGURE 4.18: Normalized $d^2$ plotted versus time for different size ratio, (a) for leading droplet and (b) for trailing droplet

due to two important factors. First, increase in R means increase in droplet volume that ultimately delay the evaporation. Second, evaporation of the leading droplet forms a buffer layer as part of a thermal protection in its back end. With

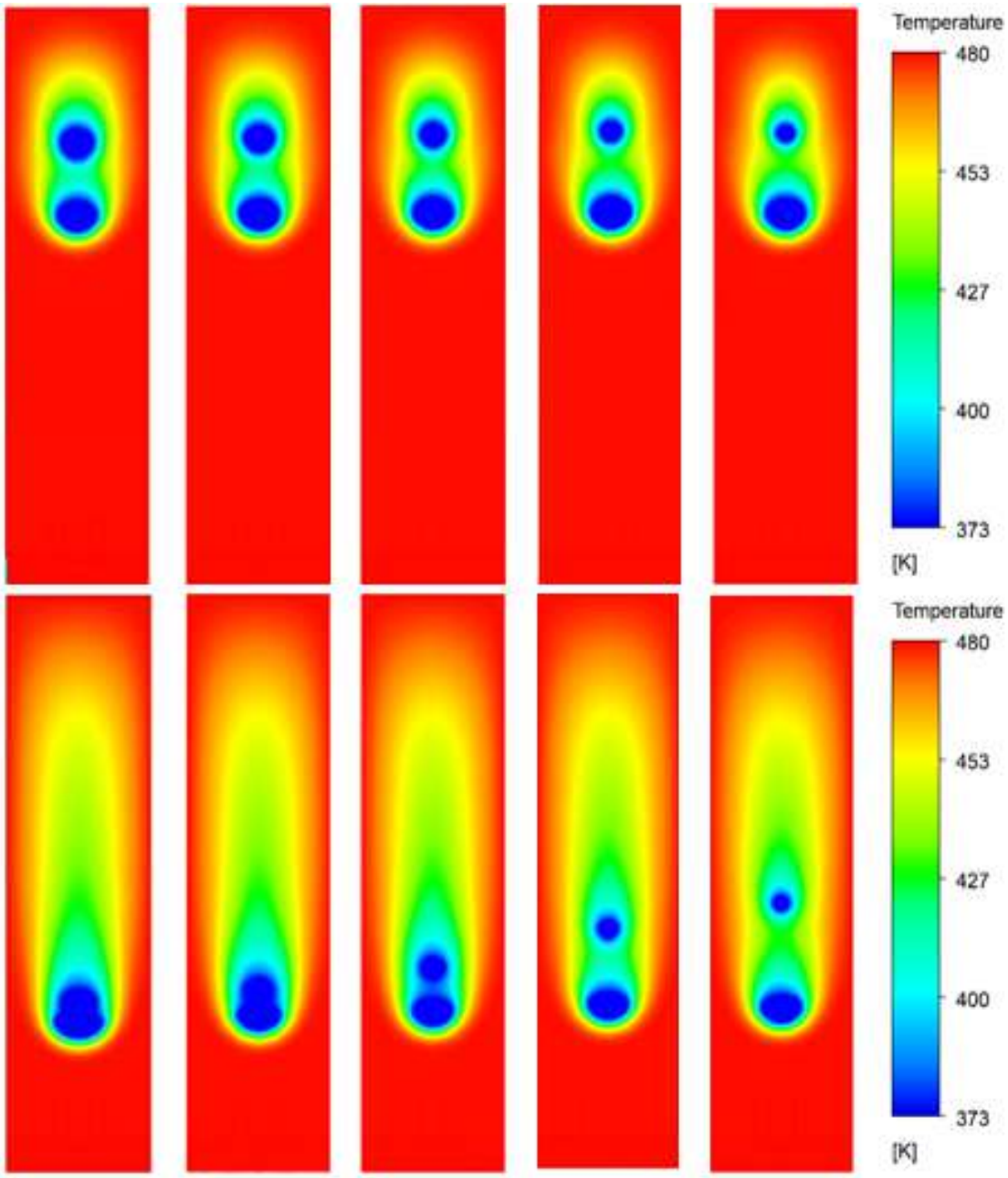


FIGURE 4.19: Contour plots of Temperature (top row) at fixed time $\tau$ =3 and (bottom row) at fixed time $\tau$ =9, showing the evaluation for an evaporating droplet (from left to right) at size ratio 0.9, 0.8.0.7, 0.6 and 0.5

decrease in R effect of this buffer layer is also minimized it can be seen in Figure 4.19 that enhance the evaporation of the trailing droplet.

Figure 4.20 show the influence of size ratio on the velocity of leading and trailing droplets. It is observed that the velocities of the leading droplet is not affected by the size ratio until the coalescence happen. While, the velocity of the trailing droplet vary non linearly. Increase in size ratio results in escalation in velocity due

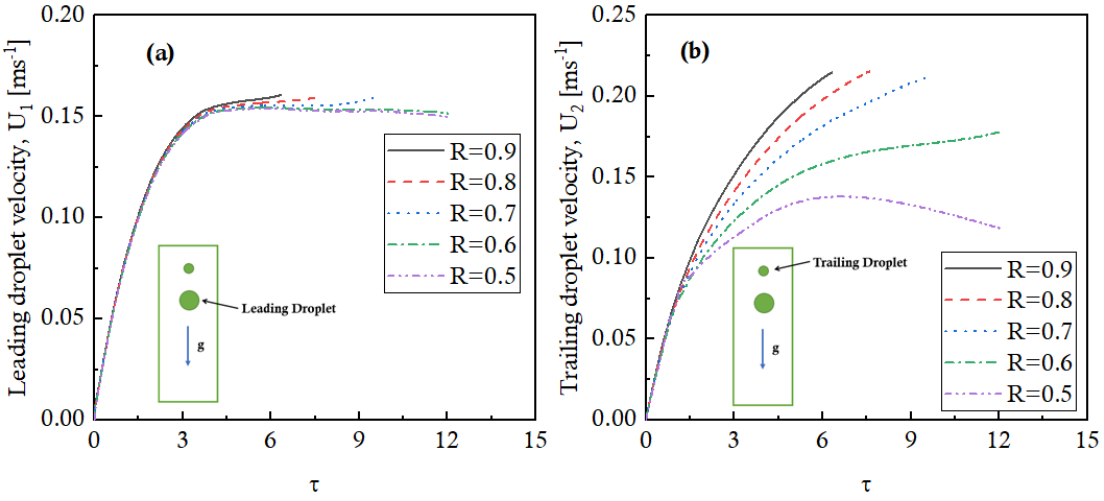


FIGURE 4.20: Velocity plotted versus time for different size ratio, (a) for velocity leading droplet and (b) for trailing droplet

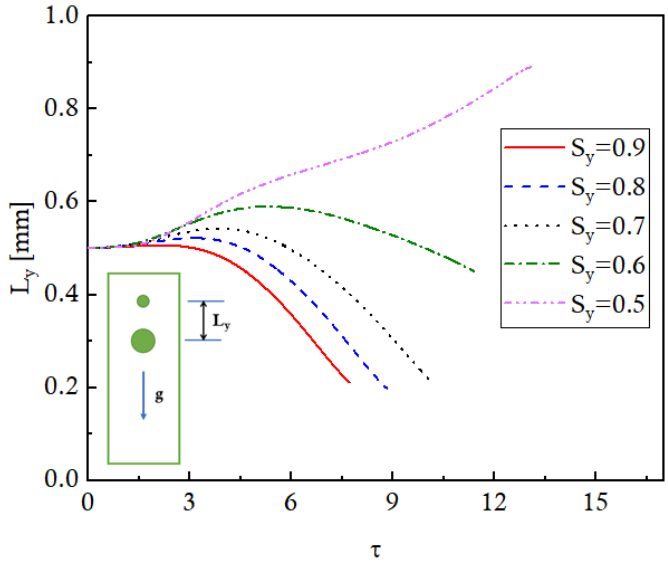


FIGURE 4.21: Effect of size ratio R on the distance $L_y$ between the centroids of two drops

to increase in mass of the droplet. Nonlinear variation in velocity cannot be the result of only inertial force but evaporation also plays a decisive role. It is noted that first droplet accelerates due to inertial forces and with the intensification of evaporation the accelerations of droplets decreases.

For a high R=0.9, reasons for early coalescence are explained in Figure 4.19 and 4.21. First with the increase of R distance between droplets decreases, leaving a small gap for the trailing droplet to evolve. By comparing the velocity fields as shown in Figure 4.20 (a) and (b) one can find that at larger R the velocity

of trailing droplet becomes stronger. On the other hand for R=0.5 as shown in Figure 4.21 the distance between the droplets increases. A smaller R means a lower volume for trailing droplet due to which it cannot accelerate much as compared to leading droplet.

### 4.4.3 Effect of the Arrangement Pattern

To study the effect of big-small and small-big arrangement pattern on the evaporation and coalescence of the leading and the trailing droplets, we fix the initial distance ratio $S_y$ =4 and size ratio R=0.5. Normalized $d^2$, droplet velocities, and distances between them considered as important output parameters.

For the small-big and big-small arrangement cases, the normalized $d^2$ is plotted

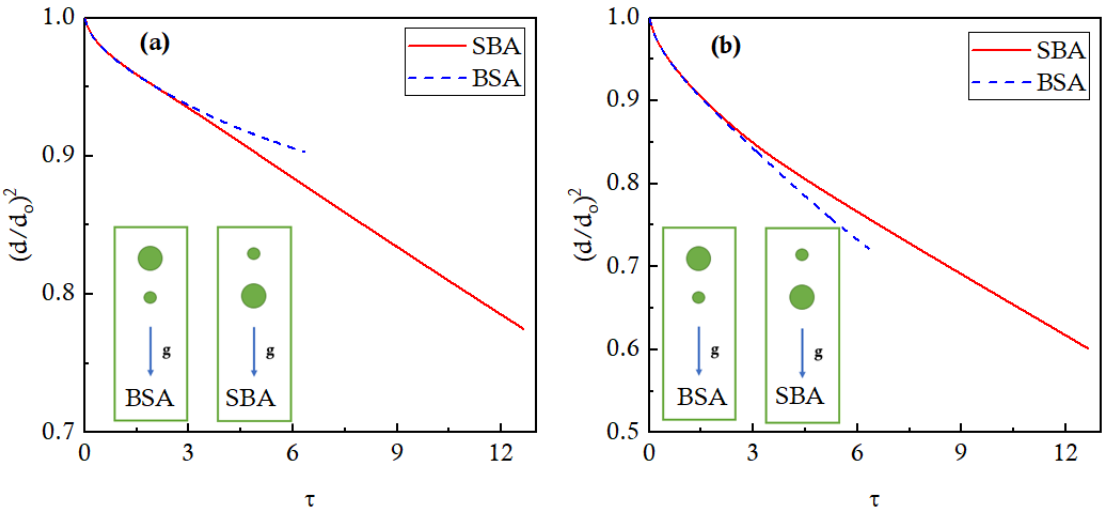


FIGURE 4.22: Normalized $d^2$ plotted versus time for different SBA and BSA (a) for big drop and (b) for small drop

as shown in Figure 4.22 for both big and small drops. It is observed that in SBA, when big drop that is leading drop starts to move, as shown in Figure 4.23 (top row) its front end is in contact with the high temperature of 480 K until it hit the wall and its backside form a buffer layer that decelerate the evaporation of the trailing droplet. On the other hand, for case BSA it is seen in Figure 4.23 (bottom row) that for the big drop that is trailing drop when droplet starts to move its front end contact are in contact with buffer layer that is less than the temperature of 480 K. The above-mentioned phenomena accelerate the evaporation of big drop

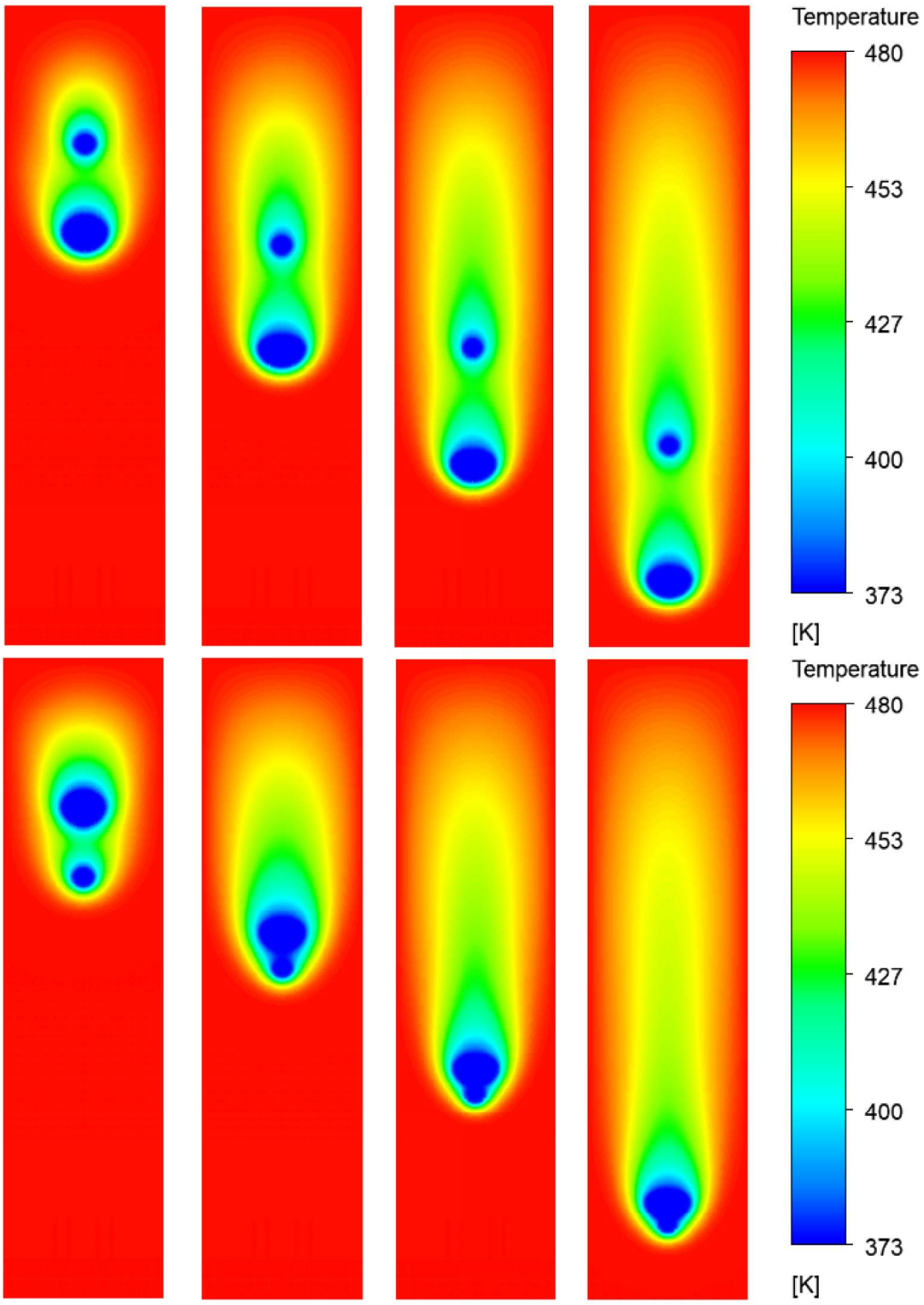


FIGURE 4.23: Contour plots of Temperature for SBA and BSA,top row representing small-big arrangement and bottom row representing big-small arrangement for $\tau$ = 3, 6, 9 and 12(from left to right)

in SBA as compared to BSA that is visible in Figure 4.22

In contrary to big drop if we see the evolution of small drop. In big-small arrangement(BSA) when the small drop is leading drop starts to move, As shown in Figure 4.23 (bottom row), its front end is in contact with a high temperature

of 480 K until it hit the wall and its backside is in contact with the thermal buffer that is not as much high temperature as compared to the front end. On the other hand for case SBA it is seen in Figure 4.23 (top row) that for the small drop that is trailing drop when droplet starts to move its both front end contact is in contact with buffer layer that is less than the temperature of 480 K. The above-mentioned phenomena accelerate the evaporation of a small drop in BSA as compared to SBA.

If we observe the overall evaporation in SBA and BSA with sizing ratio of R =0.5 as shown in Figure 4.24 that SBA arrangement enhances that evaporation as compared to BSA. In SBA more surface area is in contact with high temperature as compared to BSA before and after the coalescence of drops due to which in SBA evaporation rate is high as compared to BSA.

Velocities of leading $U_1$ and trailing $U_2$ droplets are shown in Figure 4.25 that

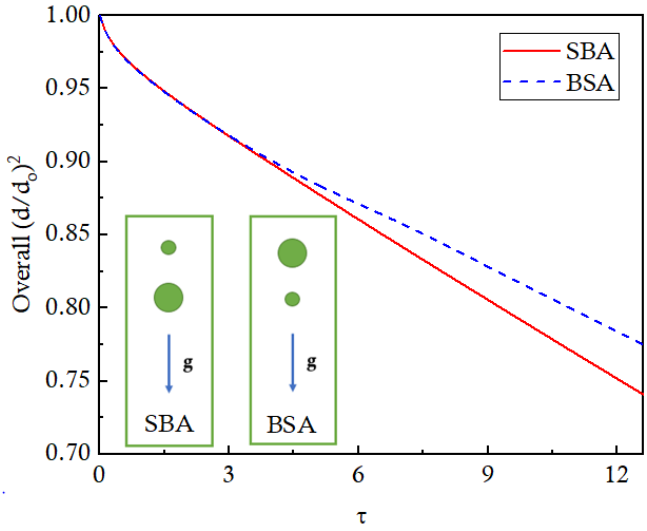


FIGURE 4.24: Influence of arrangement pattern on the overall normalized $d^2$ ($S_y$=4, R=0.5)

vary non-linearly for both arrangements. For BSA, velocity of leading and trailing droplets increases until the coalescence between droplets occurs. On the other hand for SBA velocity of the leading droplet becomes nearly constant after time $\tau$ =4 .The velocity of the trailing droplet first increase and after time $\tau$ =7.25 starts to decelerate until it hit the wall due to intensification of evaporation and its small size .

In BSA, early coalescence occur for R=0.5. By comparing the velocity fields one

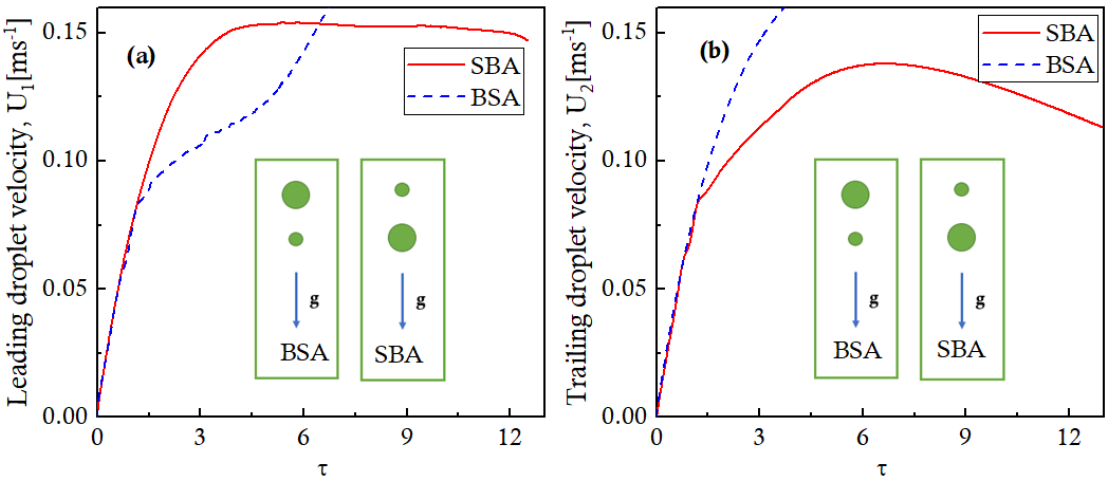


FIGURE 4.25: Velocity plotted versus time for small-big and big-small arrangement pattern, (a) for leading droplet and (b) for trailing droplet

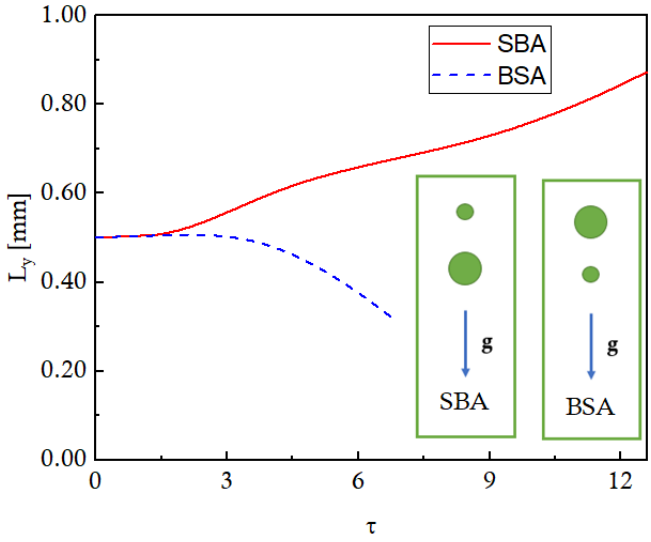


FIGURE 4.26: Effect of arrangement pattern on the distance $L_y$ between the centroids of two drops

can find that, for BSA, the trailing droplet has a large mass as compared to the leading droplet so, the velocity of trailing droplet becomes stronger and become the reason for coalescence. While for SBA no coalescence between the droplets is observed. By comparing the velocity fields one can find that for SBA the trailing droplet has a lower mass as compare to the leading droplet so, the velocity of trailing droplet is low as compared to the leading droplet that has large mass . Figure 4.26 presents the influence of arrangement pattern on distance between the droplets. In BSA distance between droplets decreases as compared to SBA in which distance between the droplets increases.

## 4.5 Closure

This chapter explained the investigation of drop-drop interaction and its effect on evaporation in detail. To understand the basic phenomena associated with the process, single moving droplet, two lateral droplets, and two inline droplets and studied to study the effect of initial distance ratio, the effect of size ratio, and arrangement pattern. The next chapter reports the numerical investigation of droplet impingement on the heated wall.

# Chapter 5

# Evaporation Dynamics during Drop-Wall Interaction in Vapor Medium

This chapter provides the details of the numerical simulation results of drop-wall interaction in a vapor medium. Even though the studies on drop-wall interaction were conducted in past, the underlying physics is not yet fully understood. In addition, the effect of impact velocity, droplet size, wall temperature and thermal boundary layer thickness is numerically investigated to a lesser extent. The numerical procedure is first validated with the numerical and experimental observations available in the literature. The global heat flow that is an indicator of an evaporation and spread radius are the key parameters to investigate the influence of droplet size, droplet velocity, wall Temperature and thermal boundary layer thickness.

## 5.1 Numerical Solution Strategy

The mathematical model equations governing the evaporation of drop-wall interaction are numerically solved in the 2D axisymmetric domain using the commercial CFD package ANSYS Fluent 2020 R2. A pressure-based-segregated code and

Pressure Implicit with Splitting of Operator (PISO) algorithm is used to solve continuity and momentum equations. During the calculation, a QUICK scheme is employed for spatial discretization of the energy and momentum equation. To discretize the pressure equation PRESTO scheme is used. For transient formulation, a first-order implicit scheme is used. Volume fraction equations with explicit formulation are solved by using the Geo-Reconstruct scheme. Relaxation factors used for pressure and momentum equation is 0.3 and 0.7 while for body forces and energy equation relaxation factor used is 1. For the accuracy and stability of the solution convergence criteria $10\times10^{-6}$ is used.

## 5.2 Important Non-Dimensional Numbers

The important non-dimensional numbers relevant to the study are discussed below:

**Weber number (We)** is the ratio of inertial forces to the capillary forces and is found to be very effective parameter for the impact studies and is mathematically defined as,

$$We = \frac{\rho_l u_0 d_0^2}{\sigma} \tag{5.1}$$

**Reynolds number (Re)** is given as the ratio of inertial forces to the viscous forces within in a fluid and is mathematically defined as

$$Re = \frac{\rho_l u_0 d_0}{\mu_l} \tag{5.2}$$

**Jakob number (Ja)** is a non-dimensional number representation of the ratio of sensible and latent heat of vaporization and is mathematically defined as

$$Ja = \frac{C_{p,g}(T_{wall} - T_{sat})}{h_{lg}} \tag{5.3}$$

**Bond number (Bo)** is defined as a ratio of body forces to the surface tension forces and is given as

$$Bo = \frac{\rho_l g d_0}{4\sigma} \tag{5.4}$$

**Prandtl number (Pr)** measure momentum diffusivity compared to thermal diffusivity and is given as

$$Pr = \frac{\mu C_p}{K} \tag{5.5}$$

The **non-dimensional time**, $\tau$ is represented by

$$\tau = \frac{u_o t}{d_o} \tag{5.6}$$

where $u_0$ and $d_o$ represents the initial velocity and diameter of drop.
Similarly, the **spreading ratio** is defined as the ratio of diameter of wetted region and initial drop diameter and is mathematically represented as

$$S_p = \frac{d_{cl}}{d_o} \tag{5.7}$$

**Non-dimensional heat flow** during drop impingement is represented by

$$Q^* = \frac{6Q}{\pi \rho_l d_0^2 u_0 h_{lv}} \tag{5.8}$$

## 5.3 Verification and Validation

### 5.3.1 Evaporation of Single Droplet Impingement over a Heated Wall

A schematic of the computational domain is depicted in Figure 5.1. As only droplet deposition, i.e. without splashing, is expected, all simulations have been performed on a 2D axis-symmetric grid. The thickness of the initial thermal boundary layer is kept constant 1 mm to obtain identical thermal conditions for all cases except where mentioned. In contrast, the size of the fluid domain is scaled by the initial droplet diameter $d_0$. For wall adhesion constant static angle of $35^o$ is used.
The boundary conditions employed in the simulations are depicted in Figure 5.1. The droplet and vapour temperature outside the thermal boundary layer are set equal to saturation temperature. The solid domain is initially uniformly super

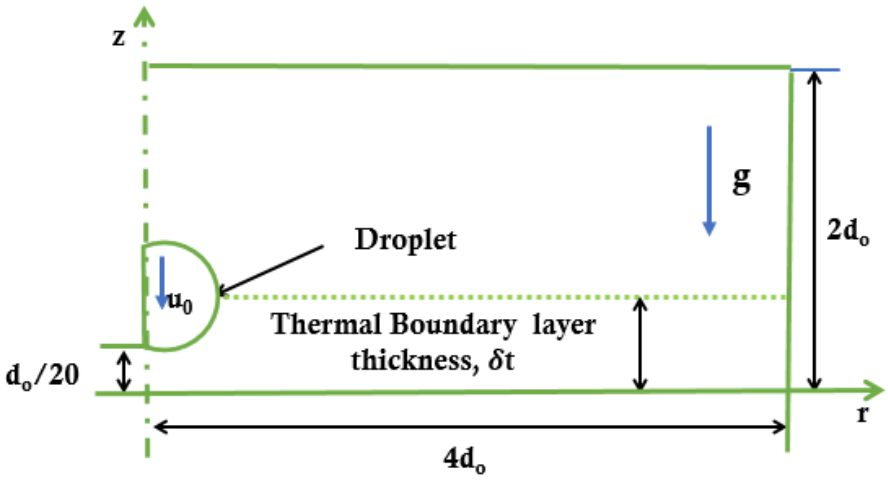


FIGURE 5.1: Schematic of the domain for drop-wall interaction

heated by $T_0 = T_{wall} - T_{sat}$. The variation of temperature in the boundary layer thickness is initialized as linear temperature profile. All outer boundaries of the domain are considered as adiabatic. For fluid, the material properties of the refrigerant FC-72 and for the solid the thermal properties of chromium are used

For validation of our numerical solution methodology, results are compared with

TABLE 5.1: Thermophysical properties of FC-72 (Perfluorohexane) at saturation pressure of 1 bar.

| **Property** | **Symbol** | **Units** | **Liquid** | **Vapor** |
|---|---|---|---|---|
| Density | $\rho$ | kg/m$^3$ | 1619.82 | 13.36 |
| Dynamic viscosity | $\mu$ | kg/m-s | 4.5306 | 9.4602 |
| Specific heat capacity | $C_p$ | J/kg.K | 1098.41 | 885.04 |
| Thermal conductivity | $K$ | W/m.K | 0.05216 | 0.00864 |
| Saturation temperature | $T_s$ | K | 329.75 | |
| Latent heat of vaporization | $h_{lv}$ | J/kg | 84515 | |
| Surface tension | $\sigma$ | kg/m$^3$ | 0.008273 | |

Herbert et,al., [12] who conducted experiments to study the evaporation dynamics of a single droplet collision onto a heated surface. Saturated FC-72 (Perfluorohexane) liquid in its vapor environment and Chromium surface were used for these studies. For simplicity all thermo-physical properties are selected temperature independent and are listed in Table 5.1. The droplet of 1.02 mm diameter was impacted with a velocity of 0.262 m/s on a wall with super heat value of 13 K which corresponds to a Weber number(We) 14 and Reynolds number(Re) 956. Later, Guggilla et al., [11] numerically validated the results of Herbert by using

same input parameters. The results obtained from the present numerical simulations are in good comparison with the experimental and numerical results for both global heat flow and spread radius as shown in Figure 5.2

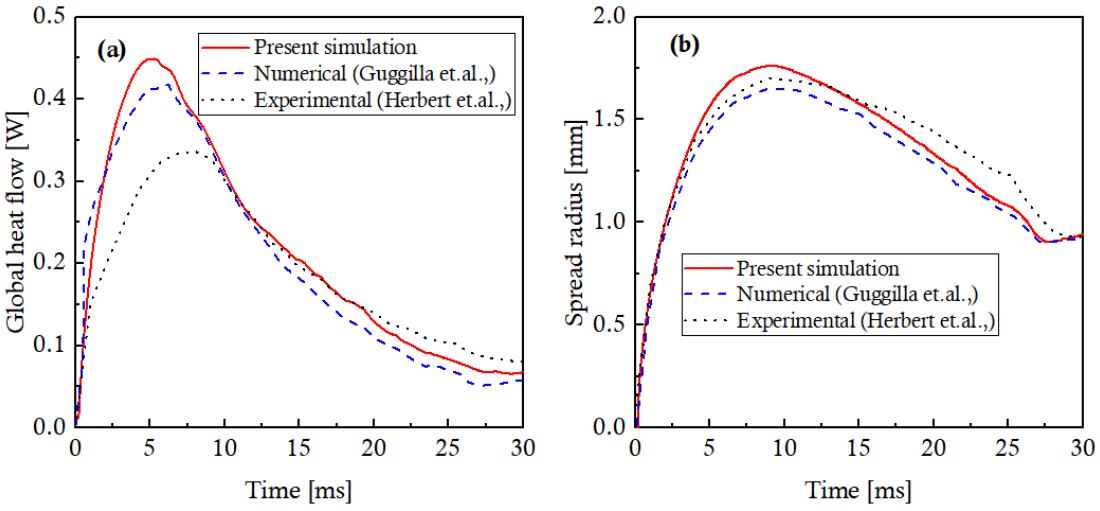


FIGURE 5.2: Validation of Present study with Guggilla et al., [11] and Herbert et, al., [12] (a) Global heat flow rate and (b) for spread radius

### 5.3.2 Grid and Time-Step Independence

To avoid numerical errors in the computational results, grid convergence studies are performed. Three different types of a structured grid named Grid 1, Grid 2 and Grid 3 with a cell size of 4, 6 and 8 micron are investigated for the domain as shown in Figure 5.1. For all three grids, the spread radius and heat flow is shown in Figure 5.3. At 5.2 ms the maximum difference between global heat flow results for Grid 1 and Grid 3 is 3.33% while, for Grid 1 and Grid 2, this difference reaches 2.1%. Similarly for spread radius as shown in Figure 5.3 (b) at 8.54 ms the maximum difference between results for Grid 1 and Grid 3 is 1.7 % while for Grid 1 and Grid 2 this difference reduces to 0.8 %. Therefore, Grid 3 with cell size 6 micron is chosen for the current study.

To investigate the time-step size effects on the solution, comparisons of the courant number 0.1,0.15 ,0.2 and 0.25 are performed as shown in Figure 5.4. With the current methodology, courant number 0.25 keeps the solution stable and accurate.

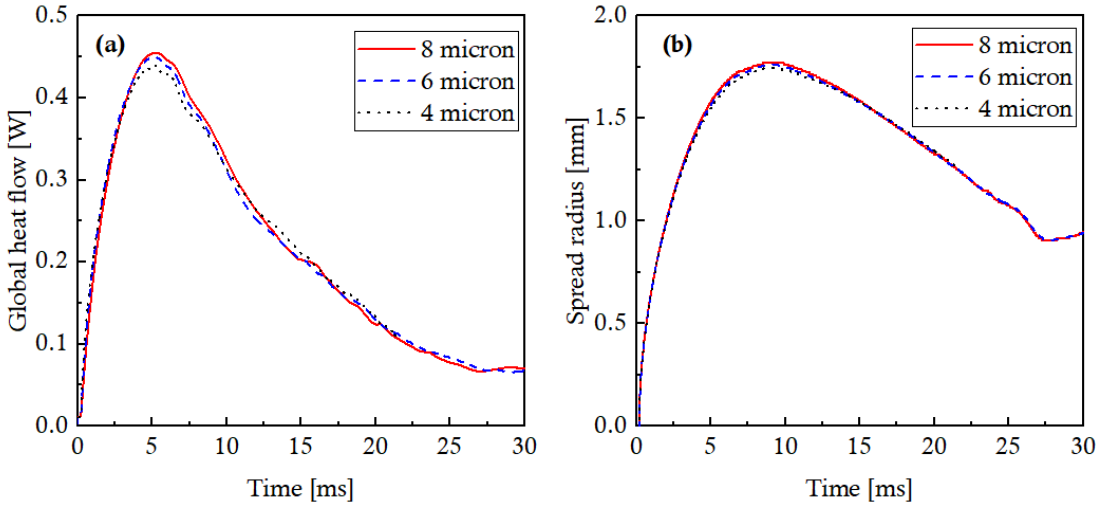


FIGURE 5.3: Result comparison for different grid resolution (a) Global heat flow rate and (b) for spread radius

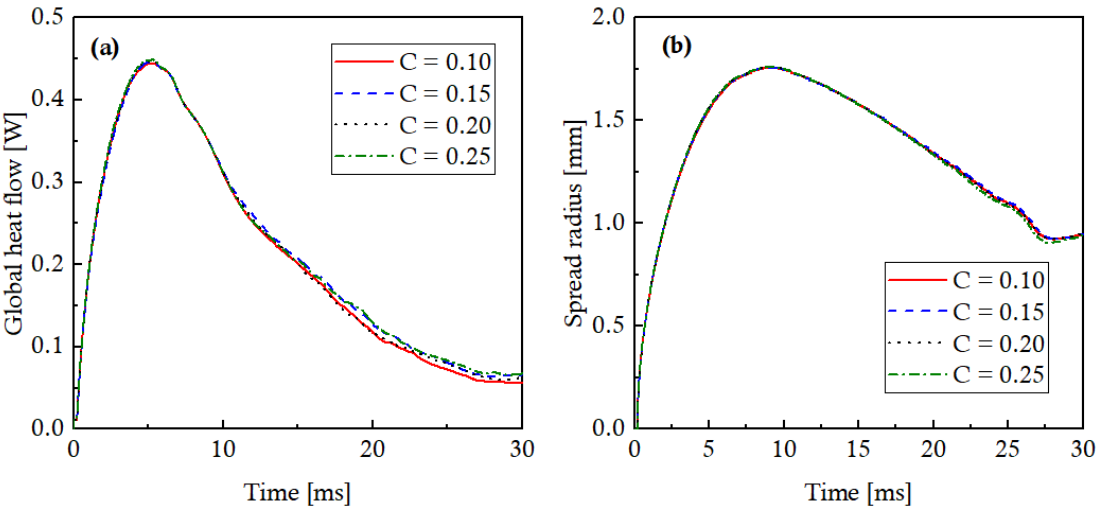


FIGURE 5.4: Result comparison for different courant numbers (a) Global heat flow rate and (b) for spread radius

## 5.4 Results and Discussion

In this section the results of the simulations for drop-wall interaction is presented. First, the simulation is performed to investigate the droplet hydrodynamics and global heat flow during the drop-wall interaction. Further this study is extended to study the effects of droplet velocity and droplet size, wall temperature and thermal boundary layer thickness during drop impingement. In this study global heat flow, spread radius, evaporative heat transfer and spreading ratio are considered targeted parameters.

### 5.4.1 Droplet Hydrodynamic Behavior

The overall droplet impact on hot solid surface can be categorized in to three phase: (i) advancing(spreading), (ii)receding and (iii) sessile droplet evaporation phase.

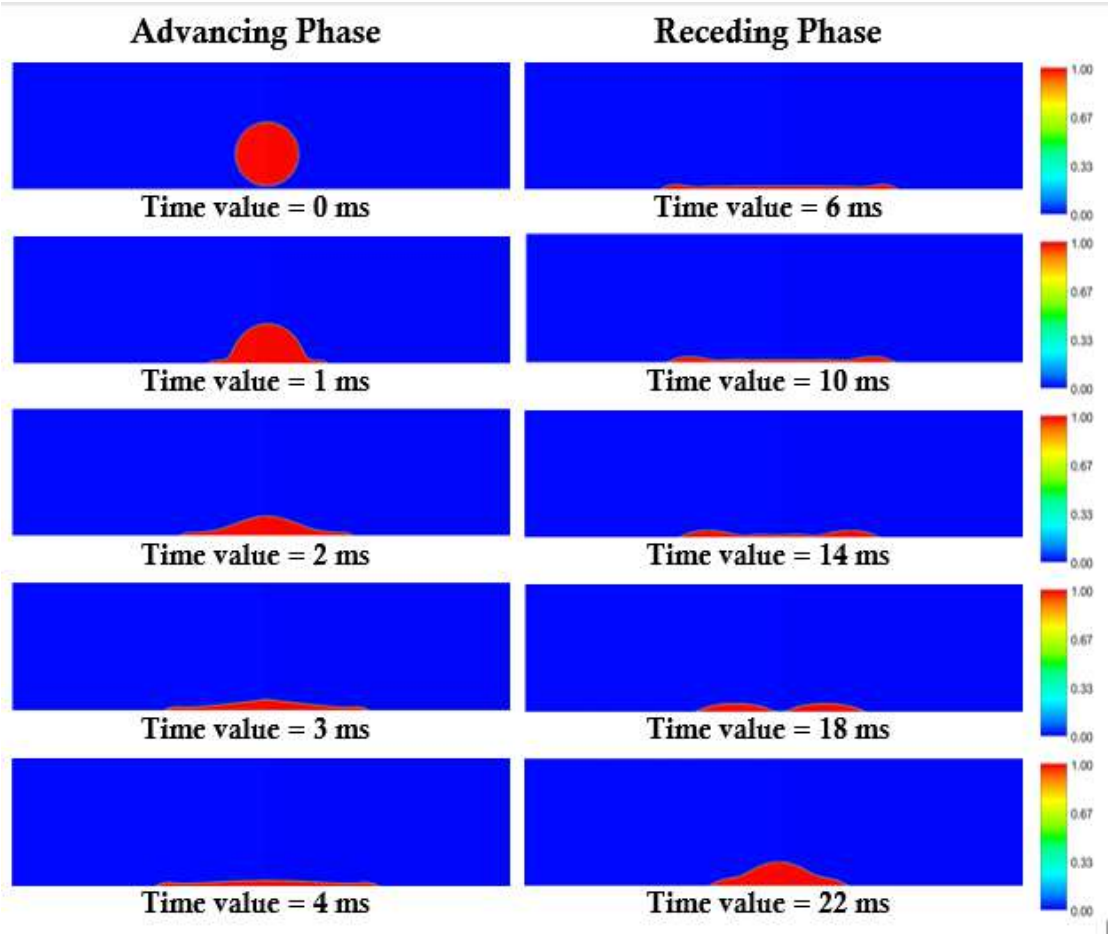


FIGURE 5.5: Contours plots of volume fraction, Left column representing advancing phase and right column for receding phase at different time intervals

Figure 5.5 represents the contours of volume fraction for advancing and receding phase. Left column correspond to advancing phase whereas, the right column represent the contours of volume fraction during receding phase at different time intervals during the droplet impingement. From simulation it is observed that during the spreading phase, the contact line of drop is moving radially outward energy. The contact line motion of fluid is dominated by inertial forces. When the drop spread reach to its maximum then drop starts to retract. This phase is known as receding phase. In receding phase, droplets retracts due to the surface

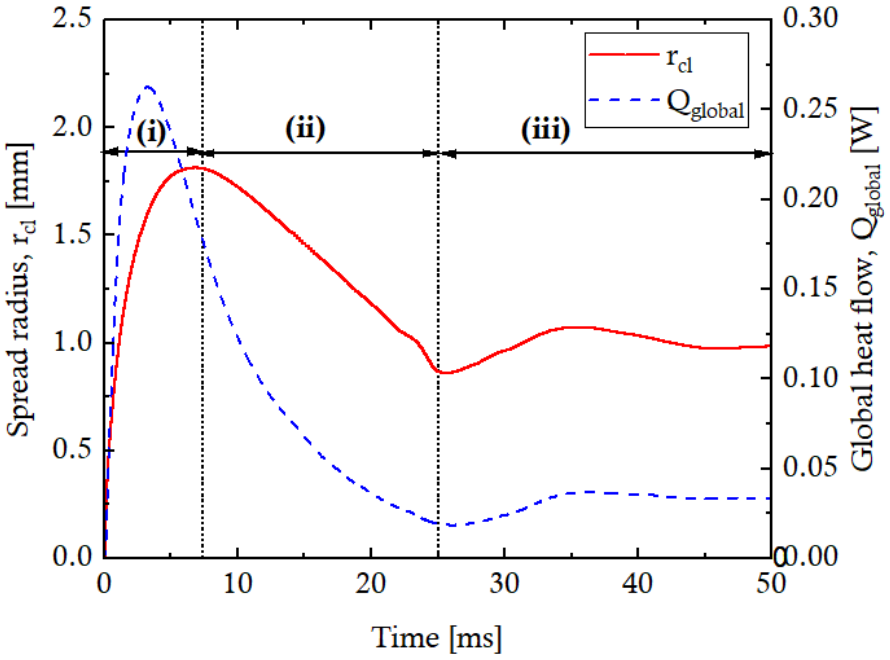


FIGURE 5.6: Temporal evolution of global heat flow and spread radius for Re=1525, We=36.7, Ja=0.08 and Bo=0.45

tension force which tries to minimize the surface area. After reaching the minimum surface area droplet oscillates until it approach to equilibrium shape which corresponds to sessile evaporation phase. Figure 5.6 represents the simulation results for spreading radius and global heat flow during drop impingement.

### 5.4.2 Global Heat Flow

When the droplet impact on hot solid surface, heat is transferred to droplet from wall and thermal boundary layer by means of conduction, convection and evaporation. The contribution of each heat transfer mechanism is different for spreading, receding and sessile phase.

Heat transfer mechanism in spreading phase is mainly from wall to the drop. In spr;8eading phase contact area between the hot wall and cold liquid increases as shown in first column of Figure 5.5 that ultimately lead to increase of heat transfer as shown in Figure 5.6. During the receding phase contact area of drop with wall starts to reduce and global heat flow continuously decreases until it reach to its minimum value. In receding phase, mainly heat is transported to liquid

droplet is from the superheated thermal boundary layer. During the sessile drop evaporation phase, the heat transport takes place mainly by evaporation.

### 5.4.3 Effect of Droplet Velocity

To study the effects of the droplet velocity on heated surface, we compare various impact velocities ranging from 0.325 to 0.575 m $s^{-1}$. Droplets start to move with the initial velocity $u_0$. Global heat flow and spread radius are considered as important and continuously calculated.

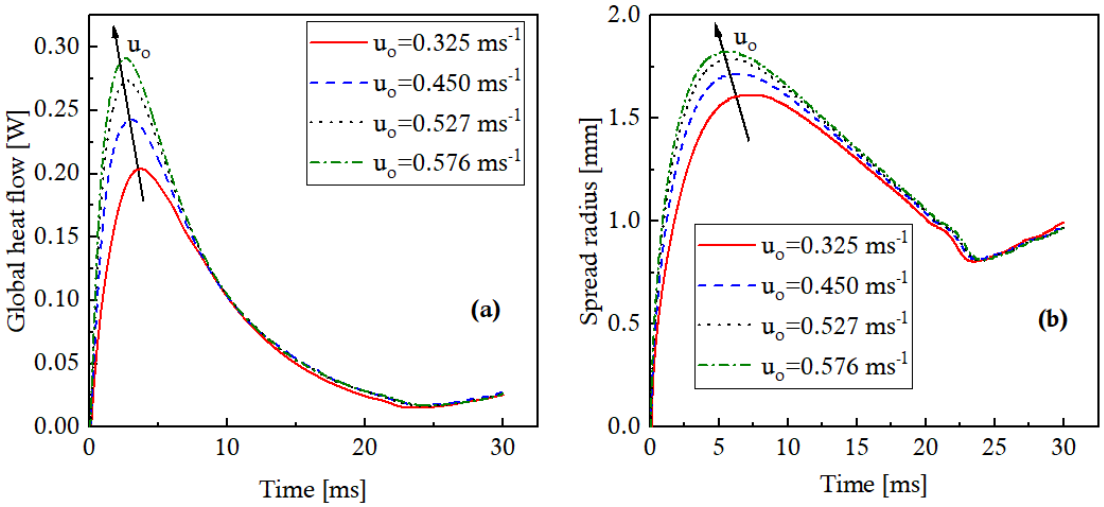


FIGURE 5.7: Results comparison for various impact velocity (a) Global heat flow and (b) for spread radius

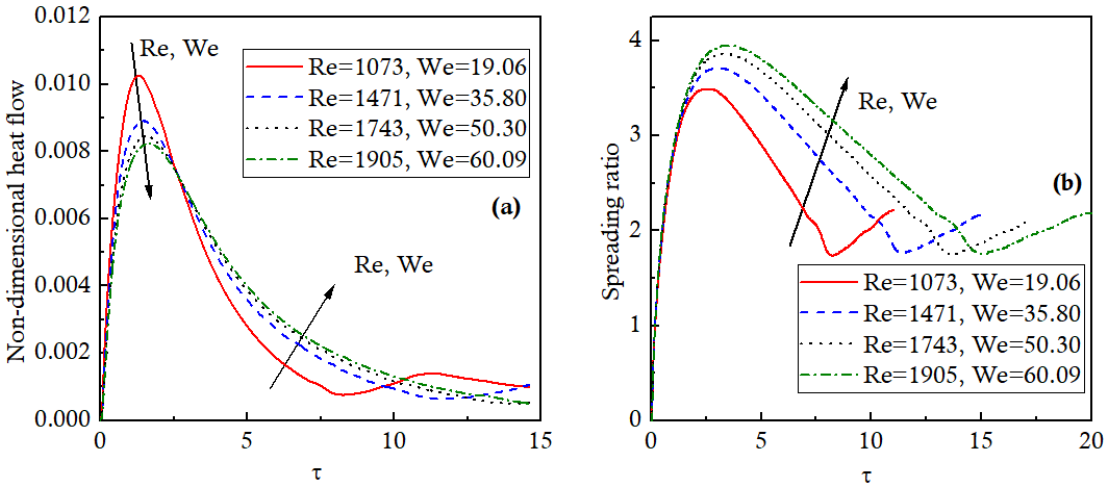


FIGURE 5.8: Results comparison for various Re and We numbers (a) Non-dimensional heat flow and (b) for spread radius

Simulation results presented in Figure 5.7 show that decrease in impact velocity results in increase in the spreading phase and decrease the spread radius. The main reason that leads to decrease in spread radius with the decrease of impact velocity is because of its lower kinetic energy. It can also be observed that receding phase is also directly proportional to the impact velocity with the increase in impact velocity receding phase also prolong and vice versa. So, it is concluded that alteration in impact velocity influences the inertia forces dominating during the advancing and receding phase.In both advancing and receding phase as shown in Figure 5.7, at higher impact velocity global heat flow also reach to its maximum and follows the same trend of hydrodynamics.

Re and We numbers increase with the increase in impact velocity. Figure 5.8 show the influence of impact velocity on heat transfer and hydrodynamics in non-dimensional form. It is observed that with an increase in We and Re numbers shift the maximum spread radius to the higher non-dimensional time. This trend are inline with the numerical work of Herbert et.al., [43] and Gholijani et.al., [33].

### 5.4.4 Effect of Droplet Size

To study the effect of droplet size impacting on heated surface, we compare droplets of various sizes having diameter ranging from 0.97 to 1.60 mm. Droplets start to move with the initial velocity $u_0$. Global heat flow and spread radius are considered as important and continuously calculated.

Simulation results shown in Figure: 5.9 that an increase in size of drops also results in prolongation in the spreading and receding phase. It is also observed that increase in drop diameter increase the maximal contact radius and global heat flow that is intuitively expected with increase in drop diameter wetted surface become large that eventually delivers large heat flow.

Re, We and Bo numbers increase with the increase in drop size. Figure 5.10 shows the influence of drop diameter on heat transfer and hydrodynamics in dimensionless form. It is observed that with an increase in Re, We and Bo number, the maximum spreading ratio shift to higher non-dimensional time. Whereas, the maximum non-dimensional heat flow reduces and occur at constant non-dimensional

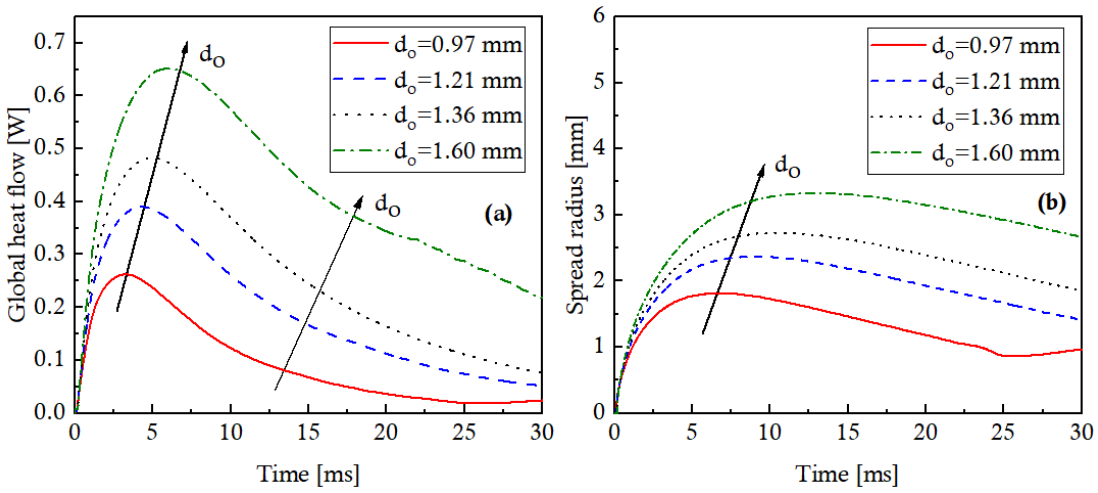


FIGURE 5.9: Results comparison for various drop size (a) Global heat flow and (b) for spread radius

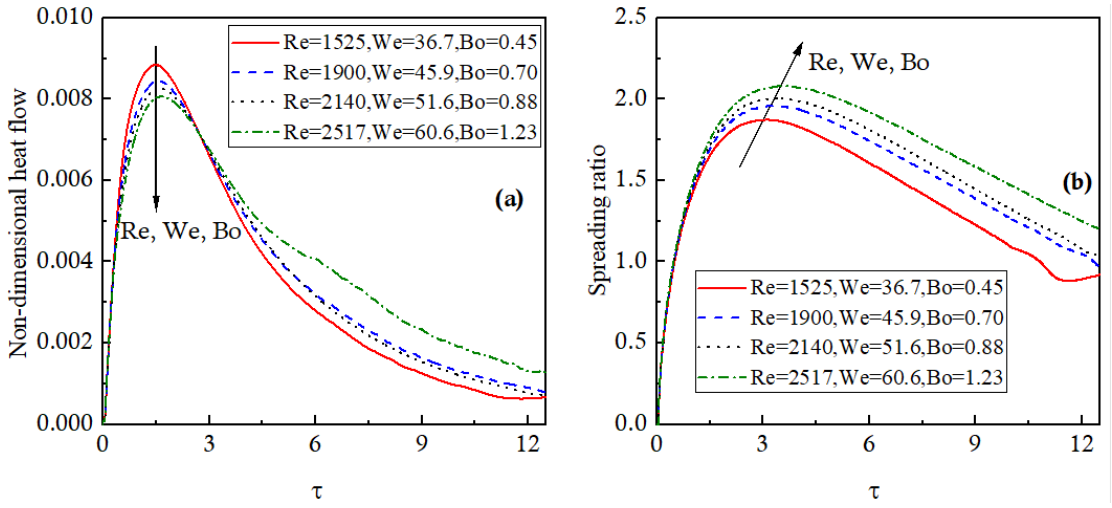


FIGURE 5.10: Results comparison for various Re, We and Bo numbers (a) Global heat flow and (b) for spread radius

time.

### 5.4.5 Effect of Droplet Wall Temperature

To study the wall temperature effect on the droplet impacted on heated surface, we compare various wall super-heated temperatures ranging from 7.7 to 16.9 K. Droplets start to move with the initial velocity $u_0$. Global heat flow and spread radius are considered as important and continuously calculated. The numerical simulation results on the influence of wall superheat ranging from 7.7 to 16.9 K on

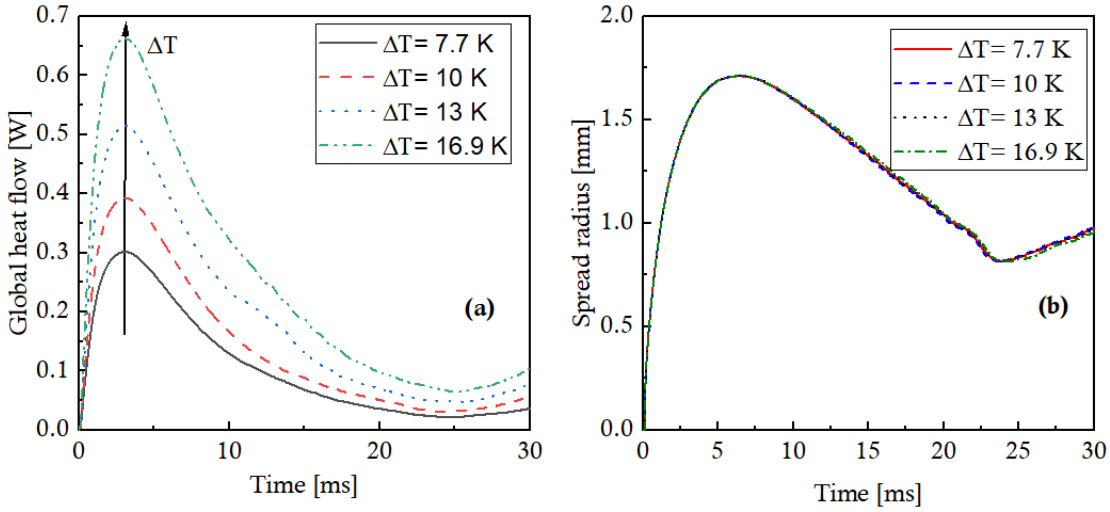


FIGURE 5.11: Results comparison for various wall temperature (a) Global heat flow and (b) for spread radius

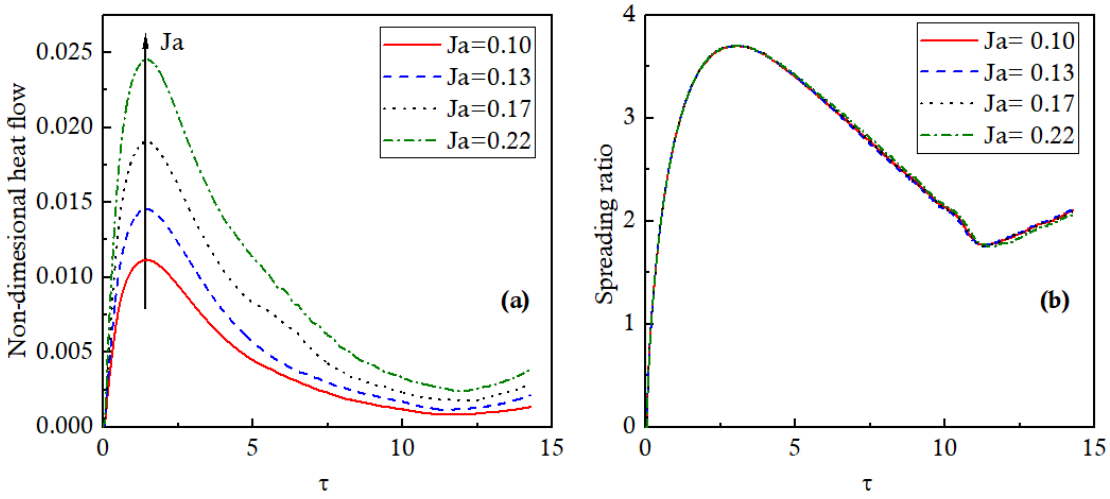


FIGURE 5.12: Results comparison for various Ja number (a) Global heat flow and (b) for spread radius

spread radius and global heat flow are illustrated in Figure 5.11. With increase in wall temperature the heat transfer from wall to droplet will significantly increase due to increase in conduction from wall to drop.

Ja number increase with the increase in wall temperature. Figure 5.12 show the influence of wall Temperature on heat transfer and hydrodynamics in non-dimensional form. It is noticed that with increase in Ja number, maximum non-dimensional heat flow increases and occur at constant non-dimensional time. No effect on spreading ratio is noticed with increase in Ja number because of the constant contact angle of surface.

### 5.4.6 Effect of Droplet Boundary Layer Thickness

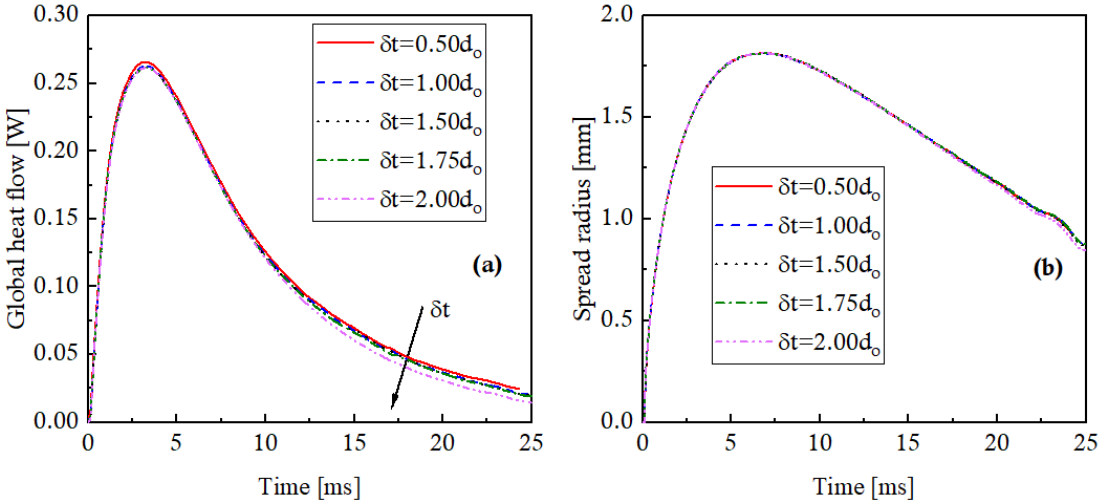


FIGURE 5.13: Results comparison for various boundary layer thickness (a) Global heat flow and (b) for spread radius

To study the effect of thermal boundary layer thickness effect on the evaporation dynamics of droplet impacted on heated surface, we compare various boundary layer thickness $\delta t$ ranging from $0.5d_0$ to $2d_0$. Droplets start to move with the initial velocity $u_0$. Global heat flow and spread radius are considered as important and continuously calculated.

Figure 5.13 shows simulation results that with increase in boundary layer thickness no effect on hydrodynamics of droplet is noticed while a negligible negative effect is noticed on heat transfer during the receding phase. When the droplet is in advancing phase mainly heat is transferred to the drop by wall.As drop retracts convection from vapor to drop surface become important and effect of thermal boundary start to visible.

## 5.5 Closure

This chapter deals with the numerical modeling of droplet impact over a heated surface and the effect on its global heat flow and spreading radius. To understand the basic phenomena associated with the process, it is compared with the single droplet impact over a heated surface and extended to study the effect of wall

temperature, droplet velocity, droplet size and thermal boundary layer thickness. From study it was found that higher wall superheats, higher impact velocities, or larger drop diameters results in increasing heat flow after the impact. With the increase in boundary layer thickness, a negligible decrease is noticed on heat transfer during receding phase.

# Chapter 6

# Conclusion and Future Work

The evaporation during the drop-drop and drop-wall interaction in hot vapor medium is of high technical importance in many industrial and technical application, in particular of spray cooling, spray drying and fire suppression. A numerical study is performed for a detailed insight into the evaporation phenomena occurring due to drop-drop and drop wall interaction and its effect on droplet evaporation. The conclusions of the study is summarized into following key points.

- It is observed that in inline configuration evaporation of leading droplet creates a buffer layer behind it, which creates condition for decreasing the heat-up and evaporation rate of trailing droplet. Hence, leading droplet evaporates faster as compared to trailing droplet.
- It is observed that with increase in $S_y$ and decrease in R the effect of buffer layer reduced on trailing droplet and results in increase its evaporation rate.
- It is observed that decrease in $S_y$ and increase in R results in increase in velocity of the trailing droplet whereas they can hardly affect the velocity of leading droplet. Nonlinear variation in velocity cannot be the result of only inertial force but evaporation also plays a decisive role
- The decrease in $S_y$ and increase in R also intensify the velocity difference between interacting droplets, which accelerates their union.

- It is observed for size ratio R= 0.5,in small-big arrangement(SBA) overall evaporation is higher as compared to big-small arrangement (BSA). In SBA more surface area is in contact with high temperature as compared to BSA before and after the coalescence of drops that leads to increase in evaporation rate.

- It is observed that the effect of channel wall on drop evolution become insignificant when the the distance of drop centroid to its side wall is grater or equal to $10d_o$

- In drop-wall interaction, it has been concluded that global heat flow increases in both advancing and receding phase with increase in wall super-heat, impact velocity and drop size. While, with increase of thermal boundary layer thickness negligible negative effect notice on global heat flow during the receding phase.

- Similarly, in case of large drop diameter and increase in impact velocity leads to increase in larger drop footprint and increase in wall super-heat increase the temperature difference between wall and liquid drop that results in increase in global heat flow.

- Increase in drop diameter and impact velocities increase the kinetic energy of the liquid drop that ultimately leads to maximum spreading. However, no effect on maximum spread is noticed with rising wall super-heat and thermal boundary layer thickness, due to constant wettability of the surface.

## 6.1 Future Work

In drop-drop interaction further studies can be performed to investigate the influence of Morton number (Mo), Eötvös number (Eo) and Stefan number (St) number on droplet evaporation in vapor/air-vapor medium. Other than this, effect of staggered arrangement of two, three or four droplets moving in air vapor medium can also be studied.

While in drop-wall interaction, effect of droplet impacting on surface with variable

wettabilities provide a great scope for future work. Also studies on droplet impact over complex surfaces is a topic of interest in many industrial and technical applications.

# Bibliography


[1] Clayton Crowe, Martin Sommerfeld, Yutaka Tsuji, et al. *Multiphase Flows with*. Ž, 1998.

[2] Carsten Baumgarten. *Mixture formation in internal combustion engines*. Springer Science & Business Media, 2006.

[3] Ross Gunn. "Collision Characteristics of Freely Falling Water Drops: With the use of new apparatus, collisions have been photographed and classified into five basic types." In: *Science* 150.3697 (1965), pp. 695–701.

[4] J Qian and Chung King Law. "Regimes of coalescence and separation in droplet collision". In: *Journal of fluid mechanics* 331 (1997), pp. 59–80.

[5] Xing Gang Li and Udo Fritsching. "Numerical investigation of binary droplet collisions in all relevant collision regimes". In: *The Journal of Computational Multiphase Flows* 3.4 (2011), pp. 207–224.

[6] Martin Rein. "Phenomena of liquid drop impact on solid and liquid surfaces". In: *Fluid dynamics research* 12.2 (1993), pp. 61–93.

[7] Romain Rioboo, Cameron Tropea, and Marco Marengo. "Outcomes from a drop impact on solid surfaces". In: *Atomization and sprays* 11.2 (2001).

[8] Alexander L Yarin. "Drop impact dynamics: splashing, spreading, receding, bouncingâ¦". In: *Annu. Rev. Fluid Mech.* 38 (2006), pp. 159–192.

[9] Gangtao Liang and Issam Mudawar. "Review of drop impact on heated walls". In: *International Journal of Heat and Mass Transfer* 106 (2017), pp. 103–126.

[10] Muhammad Irfan and Metin Muradoglu. "A front tracking method for direct numerical simulation of evaporation process in a multiphase system". In: *Journal of Computational Physics* 337 (2017), pp. 132–153.

[11] Ganesh Guggilla, Arvind Pattamatta, and Ramesh Narayanaswamy. "Numerical investigation into the evaporation dynamics of drop-on-drop collisions over heated wetting surfaces". In: *International Journal of Heat and Mass Transfer* 123 (2018), pp. 1050–1067.

[12] Stefan Herbert, Sebastian Fischer, Tatiana Gambaryan-Roisman, et al. "Local heat transfer and phase change phenomena during single drop impingement on a hot surface". In: *International Journal of Heat and Mass Transfer* 61 (2013), pp. 605–614.

[13] George Strotos, Ilias Malgarinos, Nikos Nikolopoulos, et al. "Predicting the evaporation rate of stationary droplets with the VOF methodology for a wide range of ambient temperature conditions". In: *International Journal of Thermal Sciences* 109 (2016), pp. 253–262.

[14] Vladimir Borodulin and Mikhail Nizovtsev. "Effect of the Size of Droplets on Evaporation". In: *Interfacial Phenomena and Heat Transfer* 5.4 (2017).

[15] AE Saufi, R Calabria, F Chiariello, et al. "An experimental and CFD modeling study of suspended droplets evaporation in buoyancy driven convection". In: *Chemical Engineering Journal* 375 (2019), p. 122006.

[16] GV Kuznetsov, PA Strizhak, and RS Volkov. "Heat exchange of an evaporating water droplet in a high-temperature environment". In: *International Journal of Thermal Sciences* 150 (2020), p. 106227.

[17] Xiaodong Chen, Dongjun Ma, and Vigor Yang. "Collision outcome and mass transfer of unequal-sized droplet collision". In: *50th AIAA Aerospace Sciences Meeting including the New Horizons Forum and Aerospace Exposition*. 2012, p. 1090.

[18] Daisuke Segawa, Shinji Nakaya, Toshikazu Kadota, et al. "Effects of Droplet Spacing on Evaporation of a Cluster of 13 Fuel Droplets". In: *Transactions of the Japan Society for Aeronautical and Space Sciences,Space Technology Japan* 7.ists26 (2009), Ph_1–Ph_6.

[19] Valérie Deprédurand, Guillaume Castanet, and Fabrice Lemoine. "Heat and mass transfer in evaporating droplets in interaction: Influence of the fuel". In: *International journal of heat and mass transfer* 53.17-18 (2010), pp. 3495–3502.

[20] NE Shlegel, PA Strizhak, and RS Volkov. "Collision behavior of heterogeneous liquid droplets". In: *Microgravity Science and Technology* 31.5 (2019), pp. 487–503.

[21] NE Shlegel, PP Tkachenko, and PA Strizhak. "Collision of water droplets with different initial temperatures". In: *Powder Technology* 367 (2020), pp. 820–830.

[22] Roman Sergeevich Volkov, Geniy Vladimirovich Kuznetsov, and Pavel Alexandrovich Strizhak. "Evaporation of two liquid droplets moving sequentially through high-temperature combustion products". In: *Thermophysics and Aeromechanics* 21.2 (2014), pp. 255–258.

[23] Roman Sergeevich Volkov, Geniy Vladimirovich Kuznetsov, Jean Claude Legros, et al. "Experimental investigation of consecutive water droplets falling down through high-temperature gas zone". In: *International Journal of Heat and Mass Transfer* 95 (2016), pp. 184–197.

[24] Longbin Yang, Yazhou Shao, Yitung Chen, et al. "Numerical investigation of a burning fuel droplet pair with different spacings and sizes". In: *Combustion Theory and Modelling* 24.1 (2020), pp. 41–71.

[25] S Chandra and CT Avedisian. "On the collision of a droplet with a solid surface". In: *Proceedings of the Royal Society of London. Series A: Mathematical and Physical Sciences* 432.1884 (1991), pp. 13–41.

[26] Jungho Lee, Jungho Kim, and Kenneth T Kiger. "Time-and space-resolved heat transfer characteristics of single droplet cooling using microscale heater arrays". In: *International Journal of Heat and Fluid Flow* 22.2 (2001), pp. 188–200.

[27] M Börnhorst and O Deutschmann. "Single droplet impingement of urea water solution on a heated substrate". In: *International Journal of Heat and Fluid Flow* 69 (2018), pp. 55–61.

[28] ZeFeng Wang, Jinbiao Xiong, Weiyi Yao, et al. "Experimental investigation on the Leidenfrost phenomenon of droplet impact on heated silicon carbide surfaces". In: *International Journal of Heat and Mass Transfer* 128 (2019), pp. 1206–1217.

[29] R Simhadri Rajesh, PT Naveen, K Krishnakumar, et al. "Dynamics of single droplet impact on cylindrically-curved superheated surfaces". In: *Experimental Thermal and Fluid Science* 101 (2019), pp. 251–262.

[30] Qiang Ma, Xiaomin Wu, and Tong Li. "Droplet impact on superheated surfaces with different wettabilities". In: *International Journal of Heat and Mass Transfer* 141 (2019), pp. 1181–1186.

[31] Suhaimi Illias, Mohamad Shaiful Ashrul Ishak, Suhaila Hussain, et al. "High speed visualization and analysis of maximum spreading of water droplet during impact on hot horizontal surface". In: *International Journal of Applied Engineering Research* 11.22 (2016), pp. 10832–10837.

[32] S Ya Misyura. "Evaporation and heat and mass transfer of a sessile drop of aqueous salt solution on heated wall". In: *International Journal of Heat and Mass Transfer* 116 (2018), pp. 667–674.

[33] A Gholijani, C Schlawitschek, T Gambaryan-Roisman, et al. "Heat transfer during drop impingement onto a hot wall: The influence of wall superheat, impact velocity, and drop diameter". In: *International Journal of Heat and Mass Transfer* 153 (2020), p. 119661.

[34] Arda Cetiner, Burak Evren, Mete Budakli, et al. "Spreading behavior of droplets impacting over substrates with varying surface topographies". In: *Colloids and Surfaces A: Physicochemical and Engineering Aspects* 606 (2020), p. 125385.

[35] Zhenhai Pan, Susmita Dash, Justin A Weibel, et al. "Assessment of water droplet evaporation mechanisms on hydrophobic and superhydrophobic substrates". In: *Langmuir* 29.51 (2013), pp. 15831–15841.

[36] Murat Dinc and Donald D Gray. "Drop impingement onto a wetted surface: effects of gravity and shape". In: *Proceedings of the 10th WSEAS International Conference on Fluid Mechanics and Aerodynamics (FMA12)*. 2013, pp. 374–379.

[37] Jinliang Xu, Yuanyuan Chen, and Jian Xie. "Non-dimensional numerical study of droplet impacting on heterogeneous hydrophilicity/hydrophobicity surface". In: *International Journal of Heat and Mass Transfer* 116 (2018), pp. 951–968.

[38] Mason Marzbali and Ali Dolatabadi. "High-speed droplet impingement on dry and wetted substrates". In: *Physics of Fluids* 32.11 (2020), p. 112101.

[39] Jia-Meng Tian and Bin Chen. "Dynamic behavior of non-evaporative droplet impact on a solid surface: Comparative study of R113, water, ethanol and acetone". In: *Experimental Thermal and Fluid Science* 105 (2019), pp. 153–164.

[40] Jeremiah U Brackbill, Douglas B Kothe, and Charles Zemach. "A continuum method for modeling surface tension". In: *Journal of computational physics* 100.2 (1992), pp. 335–354.

[41] Wen Ho Lee. "A pressure iteration scheme for two-phase modeling". In: *Los Alamos Scientific Laboratory, Los Alamos, NM, Report No. LA-UR* (1979), pp. 79–975.

[42] UDF Manual. "ANSYS FLUENT 12.0". In: *Theory Guide* (2009).

[43] Stefan Herbert, Tatiana Gambaryan-Roisman, and Peter Stephan. "Influence of the governing dimensionless parameters on heat transfer during single drop impingement onto a hot wall". In: *Colloids and Surfaces A: Physicochemical and Engineering Aspects* 432 (2013), pp. 57–63.